September 2015

Applications of Optical Properties from Nanomaterials for Enhanced Activity of a Titania Photocatalyst under Solar Radiation

Jon W. Pickering
University of South Florida, jwpickering@mail.usf.edu

Applications of Optical Properties from Nanomaterials for Enhanced Activity of a Titania Photocatalyst under Solar Radiation

by

Jon W. Pickering

A thesis submitted in partial fulfillment
of the requirements for the degree of
Master of Science in Chemical Engineering
Department of Chemical and Biomedical Engineering
College of Engineering
University of South Florida

Co-Major Professor: Venkat R. Bhethanabotla, Ph.D.
Co-Major Professor: John. N Kuhn, Ph.D.
Scott W. Campbell, Ph.D.

Date of Approval:
June 30, 2015

Keywords: plasmonics, upconversion luminescence, TiO2, core-shell nanoparticles

DEDICATION

I would like to dedicate this manuscript to my wife, Nichole Pickering, for always inspiring me to be the best man I can. I have received a lot of assistance over my scholastic career, in a lot of different forms, but it was her love and compassion that gave me the endurance to complete the tasks this document reveals. I will always remember and be thankful of what she has done during my time at the University of South Florida.

ACKNOWLEDGMENTS

I would like to acknowledge the Office of Undergraduate Research for an Interdisciplinary Research Scholarship which helped purchase the LEDs in this study. I would also like to thank Ed Haller for the wisdom he passed on to me with regards to transmission electron microscopy. Lastly, I would like to thank the National Aeronautics and Space Association for use of their scanning electron microscope which was responsible for the energy dispersive spectroscopy measurements.

TABLE OF CONTENTS

LIST OF TABLES

LIST OF FIGURES

ABSTRACT

In recent years, employing advanced oxidation processes (AOPs) as a means of wastewater remediation has emerged as a promising route towards maintaining a sustainable global water management program. The heterogeneous photocatalytic oxidation process has been of particular interest due to the prospective of utilizing solar radiation as the driving force behind the degradation of pollutants. Of the photocatalyst studied to date, TiO_2 remains the most attractive material for environmental applications due to its affordability, stability, biocompatibility and high quantum yield. A key draw back however is roughly only 5% of solar radiation incident on earth can provide the energy required (3.0-3.2 eV) to generate the electron-hole pairs necessary for photo-oxidation. As a means to improve the process under solar irradiance, optical properties such as surface plasmon resonance of metallic nanoparticles and upconversion luminescence of rare earth ions have been exploited for improved light harvesting as well as the generation of more usable UV light from lower energy photons. In order to explore these phenomena and their role in the enhancement of this AOP, the photocatalytic degradation of organic dyes was studied under various conditions employing Degussa P25 TiO_2 as the photocatalyst. Ag nanocubes, Ag-Pd core-shell nanoparticles and YAG:Yb^{+3},Er^{+3} served as the dopants for the various studies which resulted in enhanced degradation rates, insight into the applicability of utilizing Yb^{+3} as sensitizing ion under solar radiation and a novel core-shell nanoparticle synthesis.

CHAPTER 1: INTRODUCTION

1.1 Photocatalysis

Advanced oxidation processes (AOP) have emerged as promising solutions to environmental issues in that the reactions involved degrade toxic organic pollutants to relatively innocuous products such as CO_2, water and mineral acids. Complete degradation of organic and biologic materials makes these AOP so attractive because other common types of wastewater treatment such as: absorption separation, reverse osmosis, or chlorination, either only concentrate it to a smaller volume or are selective in what they can remove [1]. Toxic materials are so readily degraded in AOP because of the presence of hydroxyl radicals (·OH), which are generated in a variety of different mechanisms. These different mechanisms of ·OH generation categorize the specific type of AOP. Among the variety of AOP, photocatalysis is of major interest because light, which can be freely harvested directly from the sun, provides the necessary energy to drive the reaction that occurs readily at ambient conditions [2].

There are three players in the photocatalytic process: the semiconductor, a light source, and an oxidizing agent, and for the purpose of this study, the roles will be filled by: TiO_2 as the semiconductor, a variety of artificial light sources, and dissolved O_2 as the oxidizing agent. TiO_2 has been chosen as the semiconductor material because of its low cost, wide band gap, relatively high quantum yield, biocompatibility, and stability in water [3]. To date, much work has been done to improve the photocatalytic performance

of titania, such as engineering of its surface area, crystallinity and band gap but much work is left to be done as quantum yields, the unitless ratio of reaction rate to molar photon flux, are still reported at values under 1% [4]. Such low quantum yields are observed because of the available solar spectrum on earth, only about 5% of the photons possess the necessary energy to excite an electron from titania's valance band to its conduction band which when excited, the rate at which it recombines with the valance band typically does not provide ample time for the oxidation of adsorbed water molecules to occur. A visual of this described process can be found in Figure 1

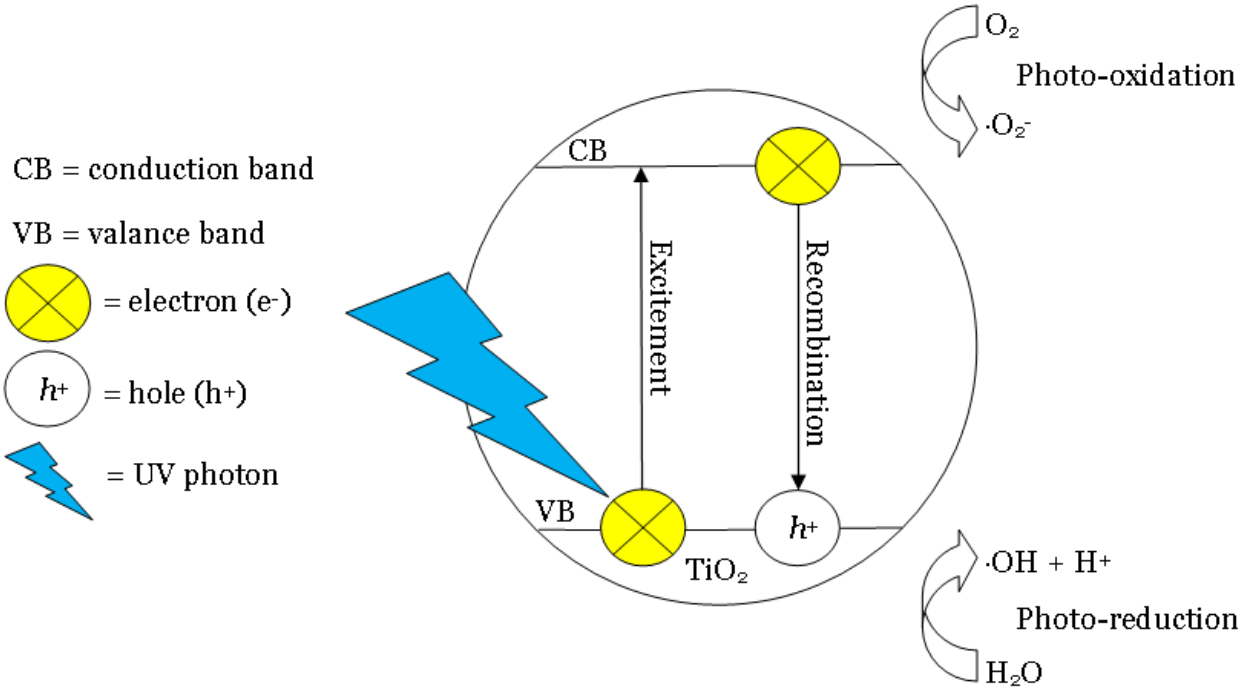

Figure 1. Example of photocatalytic cycle.

in which an ultra violet (UV) photon generates a separation of charge allowing for photo-oxidation and/or photo-reduction to occur given the electron does not recombine with titania's valance band. Photo-oxidation results in the loss of titania's

excited electron and concurrently in the reduction of the oxidizing agent. Depending on the pollutant, direct reduction can also occur as a result of photo-oxidation. This is also true at the positively charged hole in titania's valance band. Photo-reduction can be responsible for not only oxidizing water to form ·OH, but oxidation of pollutants can occur here as well. It is important to point out that the distance between the conduction and valance band is known as the materials band gap energy (E_{BG}) and is typically reported with units of eV. This E_{BG} dictates the wavelength of light that can excite the semiconductor which can be found by converting eV to a wavelength of light using the equation $E = h*c/\lambda$ where: h is Plank's constant, c is the speed of light, and λ is the wavelength of the photon.

It is the objective of this study to investigate the enhancement of titania's quantum yield under solar like radiation by employing optically active nanomaterials such as plasmonic nanoparticles (NP) and upconverting phosphors (UP) in a liquid environment. Improvement upon the quantum yield is aimed to be obtained in a multitude ways such as: localized increases in UV photon flux near the photocatalyst, improvement of electron-hole pair recombination rates due to electronic interactions of the dopants and photocatalyst, the creation of more UV photons from visible (Vis) and infrared (IR) photons from the upconversion luminescence (UCL) process, and lastly increasing pollutant concentrations near the photocatalyst surface by mixing in a material with better adsorption properties. The novelty of this study involves: a new synthetic route for Ag-Pd core-shell NP synthesis, the improved experimental procedures which extend plasmonicaly enhanced photocatalysis to the liquid phase, and the use of high-powered LEDs which produce a spectrum which provides complete

coverage of regions in which sensitized UCL occurs opposed to lasers with much tighter bandwidths.

1.2 Plasmonics

Metallic NP have been shown to have unique optical properties that are tunable throughout the UV-Vis-IR spectrum by tailoring the size, shape and composition of the NP [5]. Interactions with light occur with metallic NP due to fluctuations in charge densities at the surface of the NP. These fluctuations are called surface plasmon resonances and when this resonance matches the frequency of an incoming electro-magnetic wave, the two forms of energy couple to create what is a called a localized surface plasmon (LSP) [6]. Upon decay of the LSP, energy can be released in the form of a photon or phonon depending on the shape and composition of the NP. For this study Ag has been chosen as the metal due to its optical activity in the UV and superior scattering efficiency [7].

The shape of the Ag NP will be cubic as this shape has been shown to provide optimal enhancement to photocatalytic studies with titania as the corners and edges possess surface plasmon modes that align well with wavelengths of UV light. These geometrically specific interactions are distinguishable through UV-Vis spectroscopy as they appear as shoulders on the left handed side of the NP extinction spectrum [8]. In this study however, novelty is found in the way the NP are studied with respect to the arrangement between the NP and photocatalyst as well as investigation into the effects adding a thin shell of Pd has on the TiO_2/NP performance. It has been shown through FTDT calculations that the addition of Pd to a Ag NC should result in a reduction and

blue-shift in the peak plasmonic interactions found from the respective Ag NC core however, experimental data has not yet been reported due to difficulties associated with Ag-Pd core-shell NP synthesis [9].

1.3 Upconversion Luminescence

Rare-earth ions (RE^{+3}), found in the lanthanide series of the periodic table, have been known to have the ability to absorb multiple photons and release the energy in the form of a single, more energetic photon through a process known as excited state absorption (ESA) for some time now. The various RE^{+3} have activities that range throughout the UV-Vis-IR spectrum and it is because of their complex *f* and *d* orbitals that they are able to perform such anti-Stokes processes [10]. The UCL process can follow a multitude of pathways in which a single ion, a pair of ions or even a triplet of ions can be responsible for the emission of a photon with greater energy than the photons initially absorbed. On the left side of Figure 2 a single erbium ion (Er^{+3}) absorbs an IR photon and enters an excited state, then while still in this excited state, absorbs a second IR photon by a through ESA and ultimately releases a Vis photon. The difference in the image on the right side of Figure 2 is that initially a ytterbium ion (Yb^{+3}) absorbs an IR photon and then nonradiatively transfers the energy to a neighboring Er^{+3}, putting it in an excited state. Next, the excited Er^{+3} absorbs a secondary IR photon and releases the energy as a Vis photon which is a process called energy transfer upconversion (ETU) [10] [11].

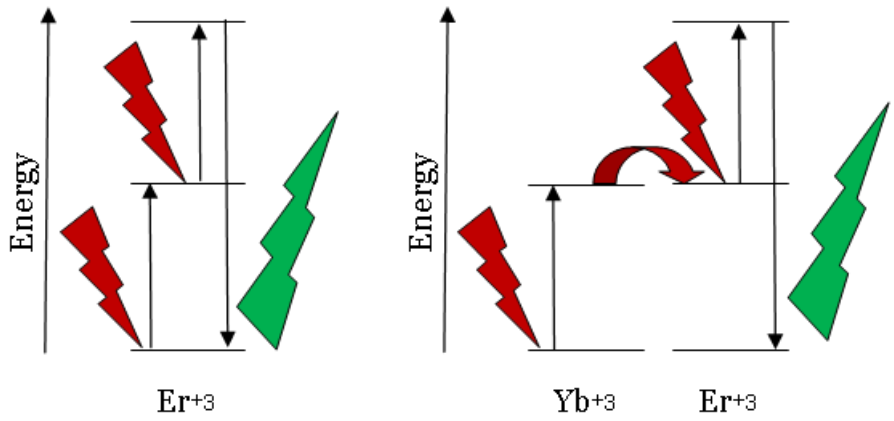

Figure 2. Visuals of single ion (left) and dual ion (right) UCL.

For this study Er^{+3} and Yb^{+3} will be co-doped in yttrium aluminum garnet, $Y_3Al_5O_{12}$ (YAG), at a constant Er^{+3} concentration in order to observe the effect of varying the Yb^{+3} concentration has on the photocatalytic enhancement obtained when the upconverting phosphor (UP) is combined with titania under varying conditions. The Yb^{+3} will be intended to act as the sensitizing ion, as shown in Figure 2 to enhance UV UCL emissions from neighboring Er^{+3}. These two RE^{+3} possess the ability of performing ETU due to an overlap in optical absorption located in the IR region so it can only be here that this form of enhancement is considered however, in the UV and Vis regions enhancement from further suppressed recombination rates and an increase in containment concentration near titania's surface from improved adsorption capabilities will also be discussed.

CHAPTER 2: METHODOLOGY

2.1 Preparation of Materials

2.1.1 Metallic Nanoparticle Synthesis

2.1.1.1 Ag Nanocubes

The Ag NC were synthesized using a polyol reduction method, following a scaled up version of that which was reported by Xia et al. [12]. 30 mL of ethylene glycol (EG) (Sigma-Aldrich, 99%) was added to a 250-mL round bottom flask and was heated under magnetic stirring in an oil bath pre-set to 150 ^{o}C. After 30 minutes of heating, 0.36 mL of 3mM NaHS (Sigma-Aldrich, hydrate) in EG was injected into the heated solution. Two minutes later, 3 mL of 3 mM HCl (Sigma-Aldrich, 36.5-38.0%) and 7.5 mL of poly(vinyl pyrrolidone) (PVP) (Alfa Aesar, 20 mg/mL MW = 58,000), both in EG, were injected into the solution. After another 2 minutes, 2.4 mL of 282 mM CF_3COOAg (Sigma-Aldrich, 99.99%) in EG was injected into the solution. During the entire process, the flask was capped except during the addition of reagents. Immediately following the addition of the CF_3COOAg solution, vapors formed in the flask and the clear solution took on a yellowish color within 2 minutes. This change in color indicated that the nucleation of Ag seeds had begun. The solution proceeded to shift colors from red, to reddish grey and finally to a greenish color with red, orange and blue undertones. After the desired time had passed from the addition of the CF_3COOAg, the flask was transferred to an ice water bath to quench the reaction. The Ag NC were washed with

acetone (VWR) once followed by three cycles of washing with ethanol (Sigma-Aldrich, 99.5%)to remove excess PVP via centrifugation. The Ag NC were then dispersed in ethanol for characterization and storage.

2.1.1.2 Ag-Pd Core-shell Nanoparticles

The Ag-Pd NP were synthesized via a successive sequential reduction process in which Ag NC were first synthesized as seeds following the previously described method. After quenching the reaction of Ag NC, the oil bath was cooled to a temperature of 90 ^{o}C to inhibit Ostwald ripening and a solution containing an appropriate amount of $PdCl_2$ (Sigma-Aldrich, 99.9) and 0.15 g of PVP (MW = 58,000) in 30 mL EG was prepared. A 1 mL sample was removed from the Ag seed solution once the solution reached room temperature to compare with the resultant Ag-Pd NP. Upon reaching the desired temperature of 90 ^{o}C, the capped round bottom flask was returned back to the oil bath and the prepared Pd precursor was added to the reaction mixture. Within the first couple of minutes the solution darkened to a slight grey-green hue and then continued to darken to a deep blue-black color irrespective of the amount of Pd added. The reaction continued under magnetic stirring for 30 minutes and was then again quenched in an ice water bath. Excess capping agent was removed following the same 4 step washing process as the Ag NC. The Ag-Pd NP were then dispersed in ethanol for characterization and storage.

2.1.1.3 TiO_2/nanoparticle Composites

In a 20 mL scintillation vial 0.4 g of AEROXIDE® TiO_2 P25 (Nippon Aerosil, 99.5%) was evenly dispersed in 10 mL of ethanol via sonication. Using a pipette,

appropriate amounts of Ag NC or Ag-Pd NP solution were added to the titania/ethanol solution and were mixed via sonication for 10 minutes. Depending on the application of the TiO_2/NP composite, the ethanol was either allowed to evaporate and the TiO_2/NP was washed once using ultrapure water (Direct-Q UV3 Millipore) or the solution was transferred to an airbrush (Paasche Airbrush Company) to be applied to microscope slides as a thin film using in lab air as the propellant.

2.1.1.4 TiO_2+nanoparticle Films

On a microscope slide, a layer of NP was repeatedly deposited via solvent (ethanol) evaporation until a desired amount of NP was obtained on the slide. The resultant layer of NP was then covered by a layer of titania via the doctor blade method. The titania slurry for the doctor method was prepared by thoroughly mixing 0.4 g TiO_2, 0.75 mL water and 0.18 mL ethanol using mortar and pestle. The film depth was controlled by applying strips of commercially available packing tape to either side of the microscope slide, creating a sub mm thick trench to which the paste was evenly spread. The layered substrate was then subjected to air drying on a mechanical shaking table for 30 minutes to avoid cracking followed by 30 minutes in an oven at 100 ^{o}C.

2.1.2 Upconversion Luminescent Materials

2.1.2.1 YAG:RE^{+3} Upconverting Phosphor

The YAG:RE^{+3} UPs were synthesized following a method similar to that which was previously reported by Hassanzadeh-Tabrizi [13]. $Y(NO_3)_3{\cdot}6H_2O$ (Sigma-Aldrich, 99.8%), $Al(NO_3)_3{\cdot}9H_2O$ (Alfa Aesar, ACS 98-102%), $Er(NO_3)_3{\cdot}5H_2O$ (Sigma-Aldrich, 99.9%) and $Yb(NO_3)_3{\cdot}5H_2O$ (Sigma-Aldrich, 99.9%) were used as the source of cations.

Appropriate amounts of the nitrate salts were dissolved in 80 mL of ultrapure water (Millipore Direct-Q UV3, >18 MΩ*cm) followed by citric acid (Sigma-Aldrich, 99.5%) (CA) and then ethylene glycol (Sigma-Aldrich, 99%) (EG) at a CA:EG molar ratio of 2:1. The solutions were then introduced into a pre-heated oil bath and were continuously stirred at 80 ^{o}C in order to dehydrate the samples and accelerate the polyesterification process. The clear gels were then placed in an oven at 100 ^{o}C for 24 h. After which, the obtained aerogels were ground and calcinated at 1000 ^{o}C for 3 h.

2.1.2.2 TiO_2/YAG:RE^{+3} Composite

Resulting powders were then combined with AEROXIDE® TiO_2 P25 (Nippon Aerosil, 99.5%) by thoroughly mixing the two compounds via mortar and pestle and 1-propanol (Sigma-Aldrich, 99.9%) followed by further calcination treatment at 500 ^{o}C for 3 h. These samples will be named TiO_2/YAG:RE^{+3} and will be distinguishable by the varying [YAG:RE^{+3}] and [Yb^{+3}] molar concentrations.

2.1.2.3 TiO_2/YAG:RE^{+3} Composite Films

On a microscope slide, a layer of TiO_2/YAG:RE^{+3} composite was deposited via the doctor blade method. The composite slurry for the doctor method was prepared by thoroughly mixing 0.4 g TiO_2/YAG:RE^{+3}, 0.75 mL water and 0.18 mL ethanol using mortar and pestle. The film depth was controlled by applying strips of commercially available packing tape to either side of the microscope slide, creating a sub mm thick trench to which the paste was evenly spread. The layered substrate was then subjected to air drying on a mechanical shaking table for 30 minutes to avoid cracking followed by 30 minutes in an oven at 100 ^{o}C.

2.2 Characterization of Materials

2.2.1 X-Ray Diffraction Spectroscopy

A Bruker, D8 Advance X-ray diffractometer was used to determine crystallinity in synthesized samples. X-Ray diffraction spectroscopy (XRD) works by measuring the diffraction angles of x-rays incident on a samples surface. The diffraction angles measured are specific to a compounds phase and crystallite size and a direct correlation between them can be made by mapping intensity vs 2 times the diffraction angle, better known as 2 theta (2θ). Due to the expansive research that is done around the world, a plethora of compounds have been analyzed and recorded, which makes identification of a proper garnet phase, and any other phases of Y-Al oxides possibly found, rudimentary. Further detail of XRD procedures and results is discussed further in chapter 4.

2.2.2 Transmission Electron Microscopy

A Philips, FEI Morgagni transmission electron microscope (TEM) was used to observe shape and size distributions of the metallic NP as well as to gain insight into any differences in morphology for the various YAG:RE^{+3} UPs. The images were obtained by transmitting a beam of electrons through a sample and capturing their interactions as they pass through. For results and images, refer to chapters 3 and 4 for NP and YAG:RE^{+3} respectively.

2.2.3 UV-Vis Spectroscopy

A Perkin Elmer, Lambda 35 UV-Vis spectrometer was used to examine the extinction spectrum of the synthesized NP as wells as to monitor the reduction in dye concentration from photocatalytic testing. The measurements were obtained using a

quartz cuvette to assure no distortion in the UV region and a scan rate of 1 nm/s to minimize noise. Results from the UV-Vis are found in chapter 3.

2.2.4 Energy Dispersive Spectroscopy

A Zeiss, EVO 50 scanning electron microscope (SEM) was used to obtain the energy dispersive spectra which were compositionally sorted out by AZtec analysis software. The chemical composition of the obtained YAG:RE^{+3} and respective composites were analyzed to gain better insight into results found from XRD. A constant Er^{+3} loading was also under investigation as it was the ion responsible for emitted UV photons due to UCL. EDS results are found in chapter 4.

2.2.5 Photoluminescence Spectroscopy

An ISS, PC1 photon counting spectrofluorometer was used to confirm UCL properties within the Vis spectrum of the YAG:Er^{+3} UP. An excitation wavelength of 488 nm was used while operating in front face mode and emissions were detected by a photomultiplier tube (Hamamatsu, R928) from 385-430 nm. Results from photoluminescence spectroscopy (PL) are located in chapter 4.

2.2.6 Diffuse Reflectance Spectroscopy

A Jasco, V-670 spectrophotometer was used to determine where the YAG:RE^{+3} UP was optically active throughout the UV-Vis-IR spectrum by diffuse reflectance spectroscopy (DRS). A spectralon reference was used as well as an integrating sphere. The bands and peaks found were used to define areas in which UCL via ESA and ETU was possible. Results and further detail can be found in chapter 4.

2.3 Photocatalytic Testing of Materials

2.3.1 Slurry Batch Reactor System

Batch reactor studies were conduction in the shallow dish, batch reactor under UV-Vis and UV radiation shown in Figure 3. The front cover of the box closed off the reactor to ambient light and was only opened to take remove samples during the reactions. Prior to conducting an experiment, ample time was given to allow for adsorption equilibrium occur via stirring the slurry in the dark. Pertinent information regarding the individual studies can be found in chapters 3 and 4.

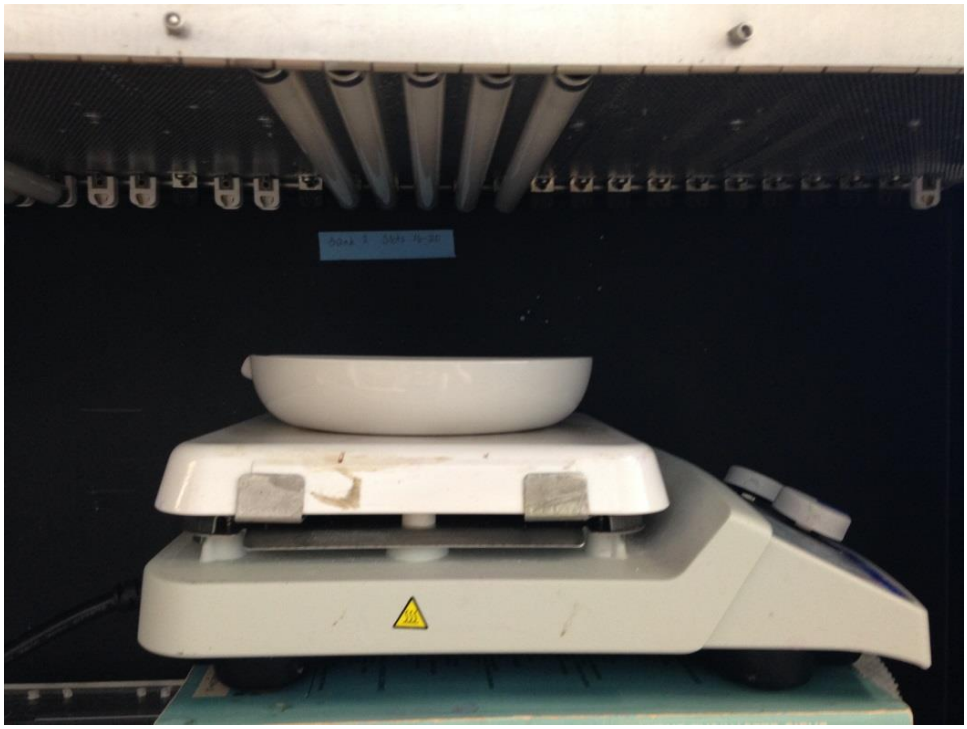

Figure 3. Image of slurry batch reactor system housed in black box.

2.3.2 Recirculating Batch Type Reactor System

Batch type reactor studies were conducted in the fabricated, stainless steel reactor on the right side of Figure 4. A glass substrate with immobilized catalyst was placed in a recess at the bottom of the reactor. A top the reactor sat the two interchangeable, high-powered LEDs which controlled by the potentiometers behind the metal from. A central pump recirculates the contaminated water that is continuously stirred in the Erlenmeyer flask to the left. The system was allowed to recirculate for 15 minutes prior to switching the LEDs on. Pertinent information regarding the individual studies can be found in chapters 3 and 4.

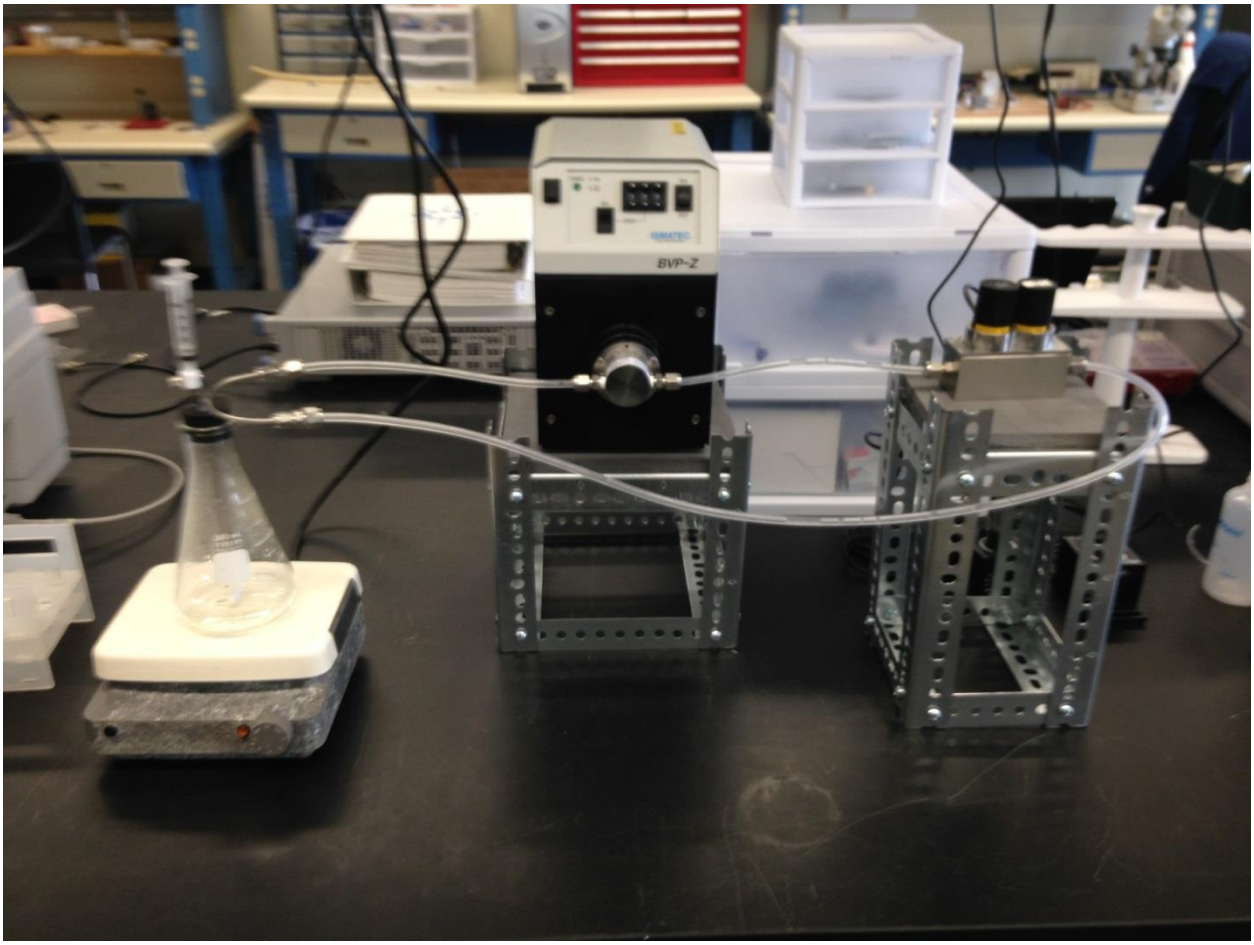

Figure 4. Image of recirculating batch type reactor system.

CHAPTER 3: PLASMONICS

3.1 Introduction

Metallic nanoparticles (NP) have been investigated heavily over the past couple of decades for their unique interactions with light. What has made these properties so interesting is that they are tunable and tailoring of size, shape and composition of NP results in the ability to select specific regions of the UV-Vis-IR spectrum that the NP interact with [14]. The interactions involve the coupling of surface plasmon resonances, which are fluctuations in charge densities along the surface of the NP, with the frequency of an incoming flux of electro-magnetic waves to form localized surface plasmons (LSP) [6]. This results in an increase of scattered photons whose frequency matched the original frequency in charge fluctuation giving rise to the notion that metallic NP possess the ability to act like a type of selectively, reflective surface. In regards to photocatalysis, the NP can by employed in a way that allows for intensified fields of light with a wavelength shorter than that of the wavelength associated with the semiconductors band gap ($\lambda \leq \lambda_{BG}$). Many reports of enhanced photocatalytic activity due to interactions between plasmonic NP and a semiconductor are resultant from experiments which involve: depositing a thin layer of plasmonic NP on a substrate, depositing or growing a semiconductor on top of the NP, submersing the substrate in a dye solution, removing the substrate and allowing it to dry in no light conditions, and then measuring change in reflectance of the remaining adsorbed dye while the substrate

is exposed to light [7] [15] [16]. While these experimental findings may have relevance to thin films used as protectant layers, they do not show relevance to wastewater remediation. A need for better designed experimental procedures is required to prove this form of enhanced photocatalytic degradation is applicable to wastewater remediation.

In this chapter we aim to improve upon the experimental design of plasmon assisted photocatalysis by both studying the arrangement of the photocatalyst and plasmonic NP and by implementing an improved reactor set-up that will subject thin film substrates to a recirculating, liquid phase environment. To achieve the differences in arrangement, a TiO_2/NP composite will be tested against a layered film arrangement in which a film of titania will be deposited on a layer of NP, which are immobilized on a glass slide, and will be referred to as a TiO_2+NP system as seen in Figure 5.

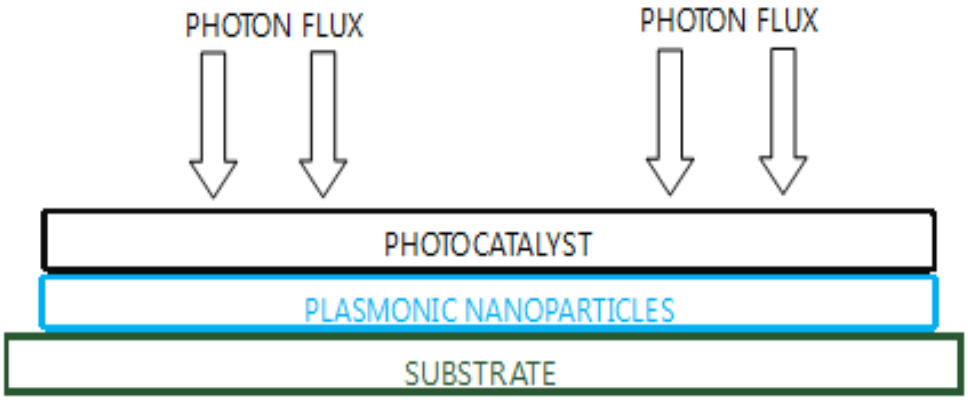

Figure 5. Depicition of the titania+NP layered arrangement.

The TiO_2/NP composites will be tested in a shallow dish, batch reactor as well in the improved reactor set-up by immobilizing it on a glass slide. It is also the aim of this study to investigate the effects of adding a Pd shell to a Ag nanocube (NC) has on the

improved performance previously achieved by implementing Ag NC to photocatalytic dye degradation studies [17]. Due to the novelty of the synthesized involved with the formation of Ag-Pd core-shell nanoparticles (Ag-Pd NP), with a Ag NC core, a series of Ag-Pd NP will be synthesized with varying Ag:Pd in order to achieve a Ag-Pd NP that retains the plasmonic properties of its core. The reason a Ag-Pd NP has not yet been reported, in which the core is cubic, is because of the rather large lattice mismatch between Ag and Pd of 4.6% and issues of Ostwald ripening associated with the in situ growth of Pd on a Ag surface at elevated temperatures [9] [18]. Upon achieving a proper Ag-Pd NP, the photocatalytic degradation of methyl orange (MO) and rose bengal (RB) bye will be studying under UV-Vis and UV conditions.

3.2 Experimental Section

3.2.1 Material Characterization

UV-Vis spectroscopy was performed by a Perkin Elmer, Lambda 35 UV-Vis spectrometer to analyze the extinction spectra of the synthesized NP. The measurements were obtained in an ethanol suspension at equal densities (g NP/mL EtOH). Images of the NP were taken using transmission electron microscopy (TEM) by a Philips, FEI Morgagni TEM in order to gain insight on particle size and shape distributions. The TEM copper grids were prepared by adding one drop of diluted NP solution, in ethanol, and then vacuum dried at 40 ^{o}C for 10 minutes.

3.2.2 Photocatalytic Testing

The photocatalytic activity of the prepared TiO2/NP composites was tested under UV and UV-Vis conditions. UV-Vis trials took place in a batch reactor, housed in a black box equipped with 5, 8W General Electric F8T5/D fluorescent bulbs (Color Rendering Index 75) providing 60 W/m^2, in which methyl orange (MO) was utilized as the model pollutant. The light intensity measurements were taken with a Li-CorPparanometer Vis (400-100 nm). The reaction volume was 100 mL and the catalyst loading was 1 g titania / L. Prior to catalyst activation, MO was allowed to reach equilibrium by magnetic stirring of the slurry in the dark for 30 minutes which resulted in a supernatant dye concentration of 200 ppm. 1 mL aliquots were removed every 30 minutes and MO concentrations were measured by UV-Vis spectroscopy. UV trials were performed in a fabricated, stainless steel batch type reactor upon which two, 410 mW Thorlabs M405L2 UV LEDs were mounted and provided 405 nm light (13 nm FWHM). Two configurations of the TiO_2-NP complex were studied in these trials: the first being a layered arrangement in which the base layer of NP, immobilized on a glass slide, were coated with a top layer of pure titania and the second being a single layer of the TiO_2/NP composite immobilized on a glass slide. Rose bengal (RB) dye was used as the model pollutant in the UV trials and UV-Vis spectroscopy was used to monitor the degradation. A switch in dyes was resultant in the realization that a positive valence charge found in MO structure, direct reduction by excited Ag NC could interfere with compared results. RB however has a neutral electronic state and direct reduction is less probable [19] [20] [21] [22]. A total reaction volume of 100 mL was used with an initial RB dye concentration of 400 ppb and 1 mL aliquots were removed every 5 or 15 minutes. A reduction in initial dye concentration was due to a difference found in absorbance vs

concentration calibration studies which were conducted to observe the limits of detection of both dyes. Apparent quantum efficiencies ($\Phi_{MO/RB}$) for UV-Vis experiments were calculated using the experimentally determined degradation rates and photon flux as follows:

$$\Phi_{MO/RB} = \frac{R_{MO/RB}\left[\frac{mol}{s}\right]}{J\left[\frac{mol}{m^2 * s}\right] * A\,[m^2]}$$

where: $R_{MO/RB}$ is degradation rate of the specific dye, J is photon flux and A is irradiated surface area. Ultrapure water was used in all photocatalytic studies.

3.3 Results and Discussion

3.3.1 Structural and Optical Characterization

Upon analyzing the extinction spectrums of the succession of synthesized Ag-Pd NP, it was found that retention of the Ag seed's plasmonic properties was not observed until a Ag:Pd of 9:1. Figure 7 (a) displays how at a Ag:Pd of 3:1, a relatively horizontal extinction line is obtained from the Ag-Pd NP due to the thickness of the Pd shell, which cannot reach over 5 nm, and the distinctive black color of the solution. At a Ag:Pd of 6:1 a small fluctuation in the extinction spectrum was observed from 326-423 nm but, there was no true peak or shape as seen in Figure 7 (b). Figure 7 (c) shows that after the addition of Pd^{+2} to the Ag seed solution a reduction and blue-shift in the peak extinction is observed, suggesting that there is in fact a layered Ag-Pd NP. It was not until a Ag:Pd

of 15:1 that the Ag-Pd NP extinction spectrum truly resembled the Ag seed's. In Figure 7 (d) a reduction in peak extinction intensity of only 10% and a blue-shift of 17 nm was found for a Ag:Pd of 15:1. Due to the high retention of both shape and intensity of the Ag seed's extinction spectrum the 15:1 Ag-Pd NP were used for photocatalytic testing. A compilation of the respective Ag seed peak extinctions, Ag-Pd NP peak extinctions and peak extinction intensity reductions can be found in Table 1.

In order for proper comparison to be made of the Ag NC and Ag-Pd NP with respect to plasmonic interactions, a batch of Ag NC was synthesized to best overlap the Ag-Pd NP extinction spectrum in the range at which photons possess the necessary energy to drive the reaction. In Figure 6 it can be seen that, opposed to the shoulders found on the Ag NC spectrum due to surface plasmon modes near corners and edges, both extinction spectrums follow a similar trend in spectrum with $\lambda \leq 410$ nm. This similarity in extinction spectrums was used to justify any enhancement found due to the addition of a Pd shell on the Ag NC core as enhancement from plasmonic interactions can be assumed to be equivalent due to matching extinction intensities at equal NP loadings.

Table 1. Sample labeling and comparison of Ag seeds and Ag-Pd NP extinction spectrums.

Sample label	Ag seed peak [nm]	Ag-Pd NP peak [nm]	Intensity reduction [%]
3:1 Ag-Pd NP	443	-	82.1
6:1 Ag-Pd NP	457	-	82.0
9:1 Ag-Pd NP	456	443	59.9
15:1 Ag-Pd NP	440	423	10.0

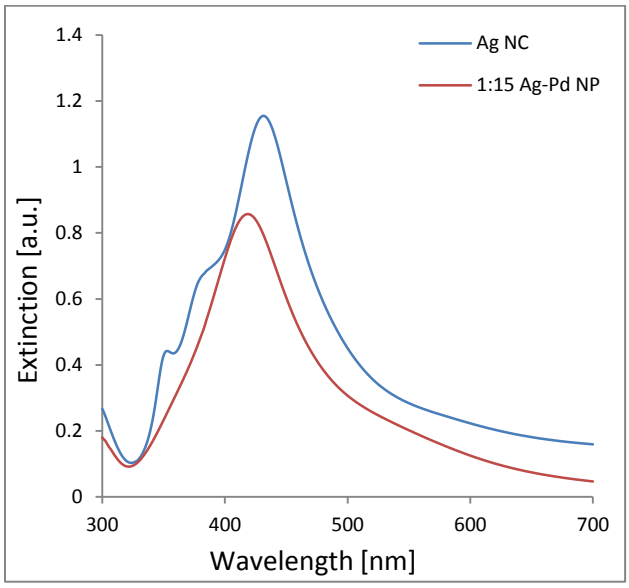

Figure 6. Extinction spectrums of Ag NC and Ag-Pd NP used for comparison in photocatalytic testing.

An estimated shape distribution of roughly 70-80% cubes, with residual particles taking on a mixture of spherical and pyramidal shapes, was determined using TEM. Selected TEM images are displayed in Figure 8 which also reveals a relatively uniform size distribution. Analysis also revealed an average shell thickness of 5 nm for the 9:1 Ag-Pd NP. This was determined by using the measuring tool on the TEM software and analyzing the shell thickness of the particles which returned planar, cross section images opposed to surface images. As mentioned previously, electronic surface properties of the Ag NC core should no longer be measurable when the Pd shell exceeds 5 nm, and given that the extinction spectrum of the 9:1 Ag-Pd NP shows minor resemblance to its Ag seed's extinction spectrum, a measured shell thickness of 5 nm is justifiable.

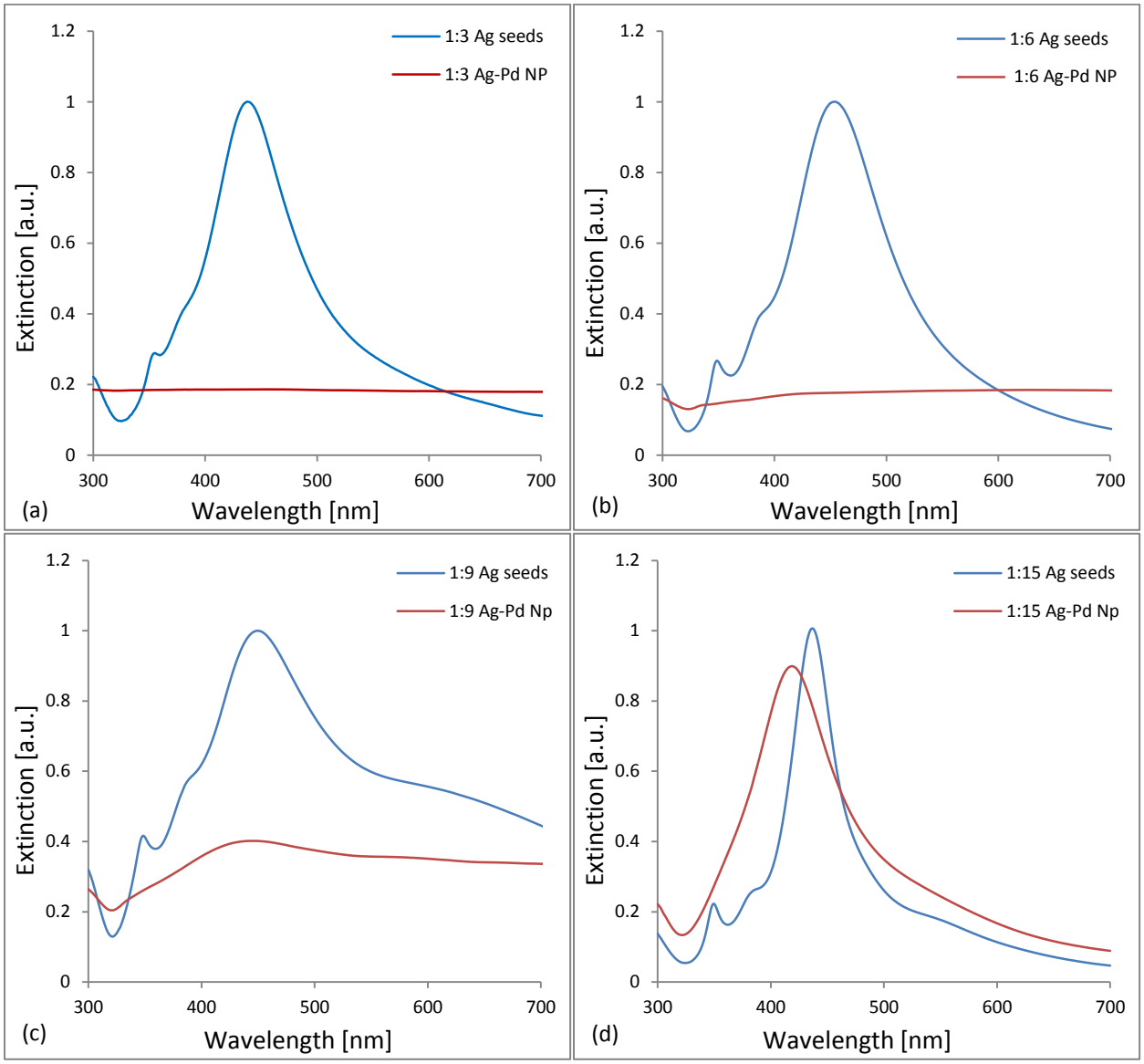

Figure 7. Extinction spectrums of the various Ag-Pd NP and corresponding Ag seeds.

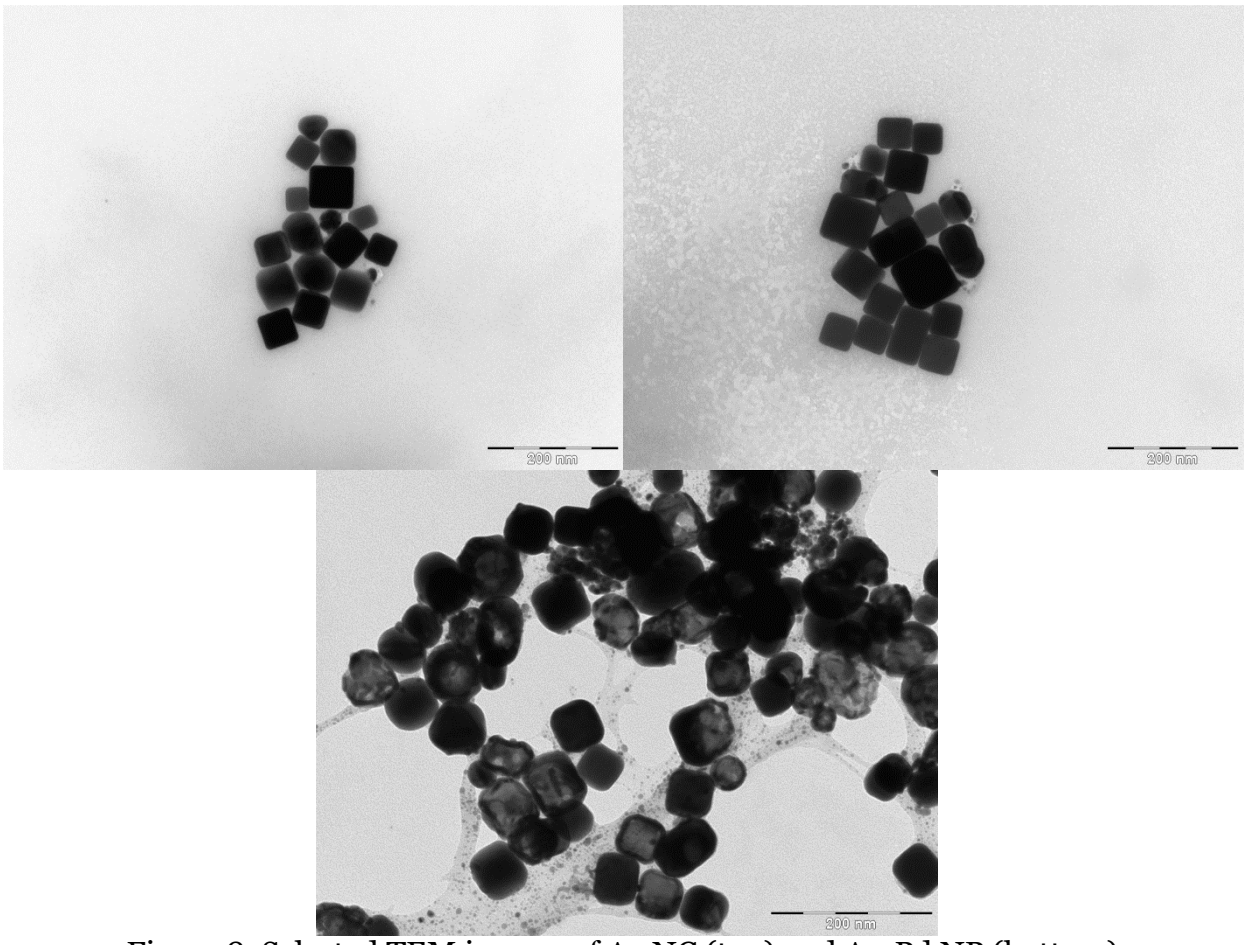

Figure 8. Selected TEM images of Ag NC (top) and Ag-Pd NP (bottom).

3.3.2 Photocatalytic Testing

The photocatalytic degradation of MO under UV-Vis conditions was performed in a shallow dish, batch reactor as a preliminary experiment to investigate the effects of titania-NP arrangement and to gain insight into the possible drawbacks of adding larger and denser metallic NP to titania in a reaction vessel more liken to ones found in typical liquid phase photocatalytic experiments [7] [15] [16]. From Table 2 it can be clearly seen that even a 0.3 wt% loading of Ag NC reduces the observed degradation rate of bare titania, -2.7 E-5 mol MO/(g*s), by 28%. Similar wt% loadings to which has been reported from methods of dried dye degradation on layered substrates, such as 1.0 and

10.0 wt%, resulted in even worse degradation rates of -1.8 E-5 mol MO/(g*s) and -1.1 E-5 mol MO/(g*s) respectively. This difference in experimental findings is indeed attributed to the titania-NP arrangement in that decorating the, engineered to be superior, P25 titania with more dense Ag NC can result in: differences in the effectiveness of mixing between titania particles in contact with Ag NC and bare titania particles, light being scattered away from the solution by Ag NC near the surface of the reaction slurry, and Ag NC covering up catalytic sites on the surface of titania particles. What was interesting however was the improvement adding a layer of Pd to the Ag NC had on the reaction rate observed by the TiO_2/[1]Ag NC composite. As seen in Figure 9, the reaction was still not superior to bare titania but it is valuable to this study that an improvement of 19% was seen by the TiO_2/[1]Ag-Pd NP composite when compared to the TiO_2/[1]Ag NC composite. Attributing factors will be discussed later.

Table 2. Φ_{MO} of TiO_2/NP composites under UV-Vis conditions.

Sample Label	Φ_{MO} [%]
TiO_2	0.0294
TiO_2/[0.3]Ag NC	0.0213
TiO_2/[1]Ag NC	0.0195
TiO_2/[10]Ag NC	0.0118
TiO_2/[1]Ag-Pd NP	0.0228

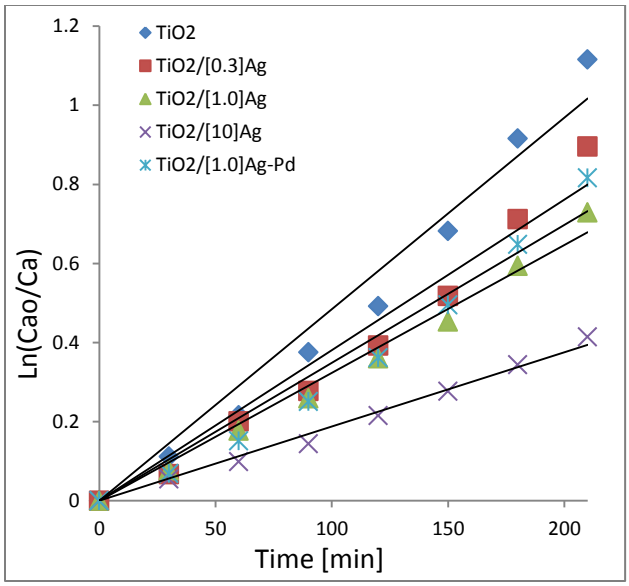

Figure 9. MO degradation under UV-Vis conditions for TiO_2/NP composites.

Table 3. k'_{RB} of TiO_2/NP composites and TiO_2+NP films under UV conditions.

Sample Label	k'_{UV} [mL/(cm²*s)]
TiO_2	0.0089
TiO_2 + Ag NC	0.018
TiO_2 + Ag-Pd NP	0.015
TiO_2/[0.05]Ag NC	0.0091
TiO_2/[0.1]Ag NC	0.010
TiO_2/[0.05]Ag-Pd NP	0.010
TiO_2/[0.1]Ag-Pd NP	0.010

In hopes of achieving improved degradation rates, an approach similar to dried dye degradations was taken in that a layered arrangement of the titania-NP system was implemented for photocatalytic testing using the improved experimental design. A transition from MO to RB dye as the model pollutant was also put into place because it has been suggested that positive and negative charges typically found on dyes offer means to complex forms of degradation and, opposed to MO, RB is neutral in solution [23]. Initially the TiO_2+NP arrangement was tested which resulted in improved

degradation rates for both TiO_2+Ag NC and TiO_2+Ag-Pd NP systems. From Figure 10 the addition of an under layer of Ag NC to the bare titania substrate doubled the degradation rate from -2.6 E-5 mol RB/($cm^{2*}s$) to -5.2 E-5 mol RB/($cm^{2*}s$) however the addition of a Ag-Pd NP under layer only resulted in an improvement to -3.4 E-5 mol RB/($cm^{2*}s$). This reduction in overall enhancement was most likely evidence that even though the Ag NC and Ag-Pd NP have similar extinction spectrums at $\lambda \leq 410$ nm, the higher scattering efficiency of Ag must have an effect on the NP layer's ability to locally intensify the flux of UV photons in the titania top layer. The fact that the interface between the Pd shell and titania particles was no longer evenly spread throughout the titania and is concentrated to one continuous titania-Pd interface also seemed to have an effect on the improvements seen in the MO experiments.

To complete the study, TiO_2/NP composites were testing in the layered film arrangement. In Table 3 at very small wt%, improved first order rate constants are found in a liquid phase, batch type reactor by the addition of Ag-Pd NP to a titania photocatalyst. The initial wt% of 0.05% Ag NC did not have an effect on the degradation rate however, at this same wt%, Ag-Pd NP improved the degradation rate to -2.9 E-5 mol RB/($cm^{2*}s$). Increasing the NP loading to 0.1 wt% resulted in an interesting outcome in that the improvement obtained by both the TiO_2/[0.1]Ag NC and TiO_2/[0.1]Ag-Pd NP composites fell within error of one another and no improvement upon the TiO_2/[0.05]Ag-Pd NP composite was observed as seen in Figure 11. It was deduced from there that further addition of NP to the TiO_2/NP composites would result in reduced degradation rates based on what was found at a loading of 0.3 wt% Ag NC in the batch experiments.

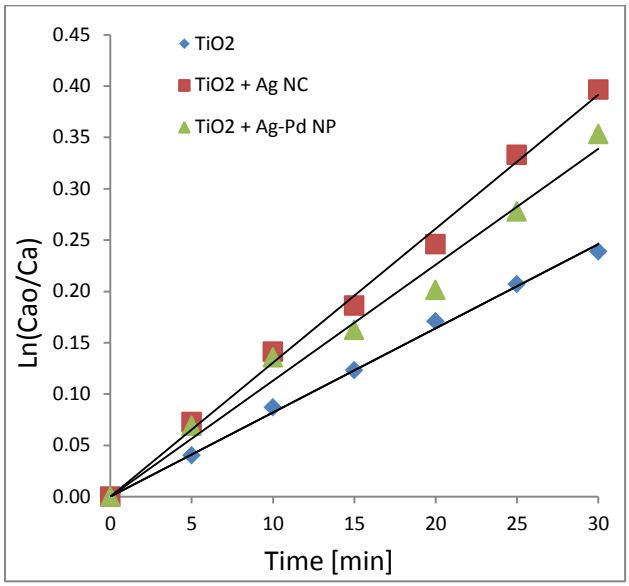

Figure 10. RB degradation under UV conditions for TiO_2+NP films.

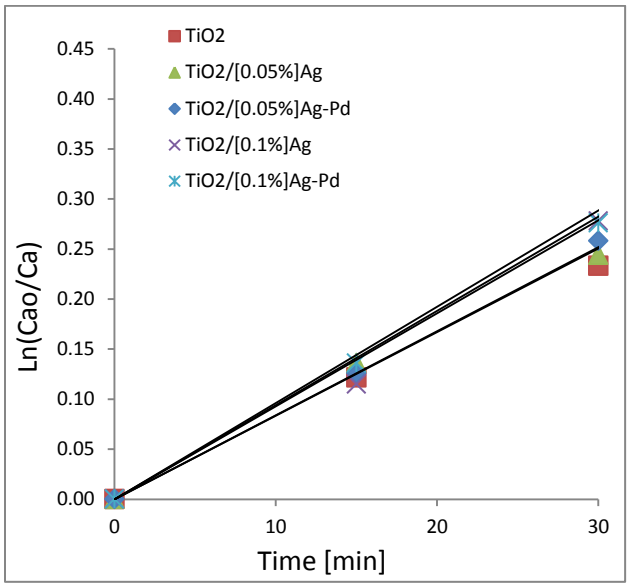

Figure 11. RB degradation under UV conditions for TiO_2/NP composite films.

3.4 Conclusions

Various loadings of Ag NC and Ag-Pd NP were studied in TiO_2/NP composites and TiO_2+NP layered systems. Experimental procedures were improved upon in that bench scale reactions were conducted in a manner more relevant to applications found in industry. Using the comparison of extinction spectrums to optimize the novel Ag-Pd NP synthesis technique, a Ag:Pd of 15:1 was determined to result in proper retention of the Ag core's distinctive plasmonic properties after addition of a thin Pd shell. Efforts were taken to best distinguish enhancement brought on due to Pd's electron scavenging properties by comparing a set of Ag NC and Ag-Pd NP which showed similar extinction trends at $\lambda \leq 410$ nm but it was found that Ag's high scattering efficiency resulted in a greater enhanced degradation rate when compared to Ag-Pd NP in a TiO_2+NP layered arrangement. To expand upon this, the two shoulders located to the left of the peak of the Ag NC's extinction spectrum in Figure 6 and 15:1 Ag seed's extinction spectrum in Figure 7 (d) are representative of distinctive surface plasmon modes located at the edges and corners of the Ag NC. However, these are not present in the 15:1 Ag-Pd NP extinction spectrum and because these shoulders appear in an area of the spectrum where all light has the potential to generate an exciton, removal of these geometrically specific plasmon modes resulted in a decrease in enhancement brought on by plasmonic interactions with light. The more interesting results were obtained from the TiO_2/NP composite experiments which took place in the batch type reactor. For the first time improved photocatalytic degradation performance was shown for a TiO_2/Ag-Pd NP composite and as a bonus, the experiments were conducted in a way that shows relevance to wastewater remediation.

CHAPTER 4: UPCONVERSION LUMINESCENCE

4.1 Introduction

Roughly only 5% of the photons incident on earth's surface possess the necessary energy to excite an electron from the valence band to the conduction band in a titania photocatalyst due to the materials wide band gap. This means 95% of the available photons are useless regardless of any measures taken to intensify the insolation on the photocatalyst surface. Research over the past couple decades has aimed to address this issue by: doping titania with carbon, nitrogen or metal ions to shift titania's band gap into the Vis spectrum, mixing titania with other metal oxides to form composites with shorter band gaps, adding sensitizing dyes that can nonradiatively transfer the energy of absorbed Vis photons to neighboring titania molecules and by doping with materials that convert Vis and IR photons to usable UV photons by a process called upconversion luminescence (UCL) [10]. All of these methods address the issue by making more of the solar spectrum available for photocatalysis however, only UCL can broaden the available spectrum past the Vis and into the IR spectrum due to the limitations associated with shifting the band gap of materials and sensitization. The enhancement of photocatalytic activity through UCL can be achieved in three manners: the first being doping of titania with rare-earth ions (RE^{+3}), the second being mixing titania with an upconverting material, and the last being the use of reflective material covered with glass doped with RE ions [24] [25] [26] [27].

In this chapter an upconverting phosphor (UP), ytterbium (Yb^{+3}) and erbium (Er^{+3}) co-doped yttrium aluminum garnet (YAG), is combined with Degussa P25 TiO_2 (P25) and is studied at varying Yb^{+3} concentrations ([Yb^{+3}]) in order to gain insight into the effectiveness the Yb^{+3} has as a sensitizer ion in the energy transfer upconversion (ETU) process under solar like radiation. The addition of Yb^{+3} into materials with Er^{+3}, be it the photocatalyst or a material mixed with the photocatalyst, results in improved photocatalytic rates throughout the UV-Vis-IR spectrum but it is unclear unto how these improved rates are achieved due to: inconsistencies in compared material band gaps from doping for a given study, reporting reaction rates under conditions which require upconversion luminescence without the presence of an upconverting ion, and neglecting to take into account all possible routes of enhancement [25] [26] [28] [29]. In order to address these issues, YAG has been chosen to be the host of the necessary RE^{+3} ions to avoid possible variations in band gaps of the synthesized TiO_2/YAG:RE^{+3} composites, [Er^{+3}] will remain constant in all variations of the UP because it is the ion which emits the UV photons due to UCL and the intensity of these emissions are highly dependent on ion concentration, and any observed photocatalytic enhancements will be discussed from all possible angles [10].

4.2 Experimental Section

4.2.1 Material Characterization

X-Ray diffraction (XRD) patterns were attained using a Bruker, D8 Advance X-ray diffractometer. Diffraction patterns were recorded from 2θ = 15-70° with Cu Kα radiation (λ = 1.5406 Å) for phase analysis and unit cell parameters. Bragg's law was

used to observe any changes in cell volume due to the cubic nature of YAG. The chemical compositions of the samples were determined by energy dispersive spectroscopy (EDS) using a Zeiss, EVO 50 scanning electron microscope (SEM) and AZtec analysis software. All measurements were obtained with a backscatter electron detector. Transmission electron microscopy (TEM) was performed with a Philips, FEI Morgagni (M268) TEM to observe and compare the microstructures of the obtained powders. The samples were prepared by dispersing the powders in ethanol via sonication and then vacuum drying a droplet on copper grids. Diffuse reflectance spectroscopy (DRS) was performed in order: to detect the areas within the Vis and IR spectrums the RE^{+3} are active and to obtain the band gap of the samples, utilizing a Jasco, V-670 Spectrophotometer. The powders were analyzed from 350-1200 nm using a spectralon reference sample. Photoluminescence spectroscopy (PL) was used to confirm upconversion luminescent properties within the Vis spectrum of the Er^{+3} at room temperature with an ISS, PC1 Photon Counting Spectrofluorometer (PC1) operating in front surface mode. An excitation wavelength of 488 nm was filtered from a 300W high-pressure xenon arc lamp using a monochromator and the resultant emission spectrum was detected by a photomultiplier tube (Hamamatsu, R928) from 385-430 nm.

4.2.2 Photocatalytic Testing

The photocatalytic activity of the various samples was determined under UV, UV-Vis and IR irradiance using the photocatalyic degradation of Rose Bengal dye (RB) as the model reaction. The UV and UV-Vis experiments were conducted using a batch reactor and 5 fluorescent light bulbs enclosed in a light box impervious to ambient light. 8W, Rayonet RPR-3500 fluorescent ‘blacklights’ provided 315-400 nm light for the UV

experiments while 8 W, General Electric F8T5/D fluorescent bulbs (Color Rendering Index 75) produced 60 W/m^2 of a 'daylight spectrum' for the UV-Vis experiments. The intensity measurements for the 'daylight' bulbs were taken with a Li-Cor Paranometer Vis (400-1100 nm). Prior to turning on the light source, the prepared catalyst and RB dye were allowed to reach equilibrium, resulting in an initial dye concentration of 200 ppb. A catalyst loading of 0.06 g TiO_2/mL was used and the initial volume of ultrapure water was 100 mL. 1 mL aliquots were removed every minute for UV experiments and every 5 min for UV-Vis experiments while keeping the final volume removed below 10% of the initial reaction volume. UV-Vis spectroscopy was used to measure the absorbance of 549 nm light by the RB dye of the removed samples which determined the degradation rate for the individual trials by a Perkin Elmer, Lambda 35 UV-Vis spectrometer. IR experiments were performed in a fabricated, stainless steel batch type reactor upon which two, 800 mW Thorlabs M940L3 IR, high-powered LEDs, were mounted and provided 940 nm light (37 nm FWHM). The prepared composite was immobilized on a glass slide and given proper time reached equilibrium with the RB dye prior to catalyst activation. The evolution of the characteristic 549 peak was again used to determine the individual degradation rates. Apparent quantum efficiencies were calculated using the experimentally determined degradation rates and photon flux as follows for UV-Vis experiments:

$$\Phi_{RB} = \frac{R_{RB}\left[\frac{mol}{s}\right]}{J\left[\frac{mol}{m^2 * s}\right] * A\,[m^2]}$$

where R_{RB} is degradation rate, J is photon flux and A is irradiated surface area. Ultrapure water (Direct-Q UV3 millipore) was used in all photocatalytic testing.

4.3 Results and Discussion

4.3.1 Structural and Morphological Characterization

Upon analyzing the XRD patterns of the YAG:RE^{+3}, it was found that a well pronounced garnet phase ($Y_3Al_5O_{12}$) of the Y_2O_3-Al_2O_3 binary system remained after incorporation of the RE^{+3}. Figure 12 exhibits how the diffraction peaks corresponding to the (420), (211), and (400) indices retained their characteristic relative maximum intensities, confirming a well-developed YAG:RE^{+3} [30]. Diffraction lines at: 2θ = 18, 29, 38 and 43 degrees appeared in samples containing an assumed mol% of $Yb^{+3} \geq 15\%$, which can be attributed to a small shift from the garnet phase to the monoclinic phase ($Y_4Al_2O_9$, YAM) [31]. A broadening of the (400) peak is observed in the sample with [Yb^{+3}] = 10% however, no clear evidence of YAM can be found. Er_2O_3 and Yb_2O_3 diffraction lines were not found in any of the YAG:RE^{+3} samples. A noticeable increase in cell volume can be seen with increasing amounts of Yb^{+3} which suggests that replacement of the smaller Al^{+3} (ionic radius = 0.535 Å) by larger Er^{+3} (ionic radius = 0.890 Å) and Yb^{+3} (ionic radius = 0.868 Å) is more likely to occur than replacement of Y^{+3} (ionic radius = 0.900 Å) [32]. XRD also confirmed there was not a phase shift in the P25 TiO_2. The morphology and size distribution of the as-synthesized YAG:RE^{+3} were investigated by TEM. A selection of the TEM images is shown in Figure 13 which displays how the UP maintained a polycrystalline appearance and particle size

distribution of 30-90 nm. It can be seen however that with increasing [Yb^{+3}], the maximum particle size remains constant but the average particle size increases.

Table 4. Labeling, dopant types and amounts and selected physical and optical properties of prepared TiO_2/YAG:RE^{+3} composites.

Sample label	Nominal content of RE^{+3} in YAG [mol%]	Nominal content of dopant [mol%]	YAG cell volume [nm^3]	Optical band gap [eV]
TiO_2	-	-	-	3.02
YAG	-	-	1.74	-
TiO_2/[5]YAG:Er^{+3}	2.0 Er^{+3}	5.0 YAG:RE^{+3}	1.74	3.04
TiO_2/[10]YAG:Er^{+3}	2.0 Er^{+3}	10.0 YAG:RE^{+3}	1.74	3.04
TiO_2/[15]YAG:Er^{+3}	2.0 Er^{+3}	15.0 YAG:RE^{+3}	1.74	3.04
TiO_2/YAG:[10]Yb^{+3},Er^{+3}	10.0 Yb^{+3} 2.0 Er^{+3}	10.0 YAG:RE^{+3} 10.0 Yb^{+3}	1.77	3.04
TiO_2/YAG:[15]Yb^{+3},Er^{+3}	15.0 Yb^{+3} 2.0 Er^{+3}	10.0 YAG:RE^{+3} 15.0 Yb^{+3}	1.79	3.03
TiO_2/YAG:[20]Yb^{+3},Er^{+3}	20.0 Yb^{+3} 2.0 Er^{+3}	10.0 YAG:RE^{+3} 20.0 Yb^{+3}	1.80	3.03

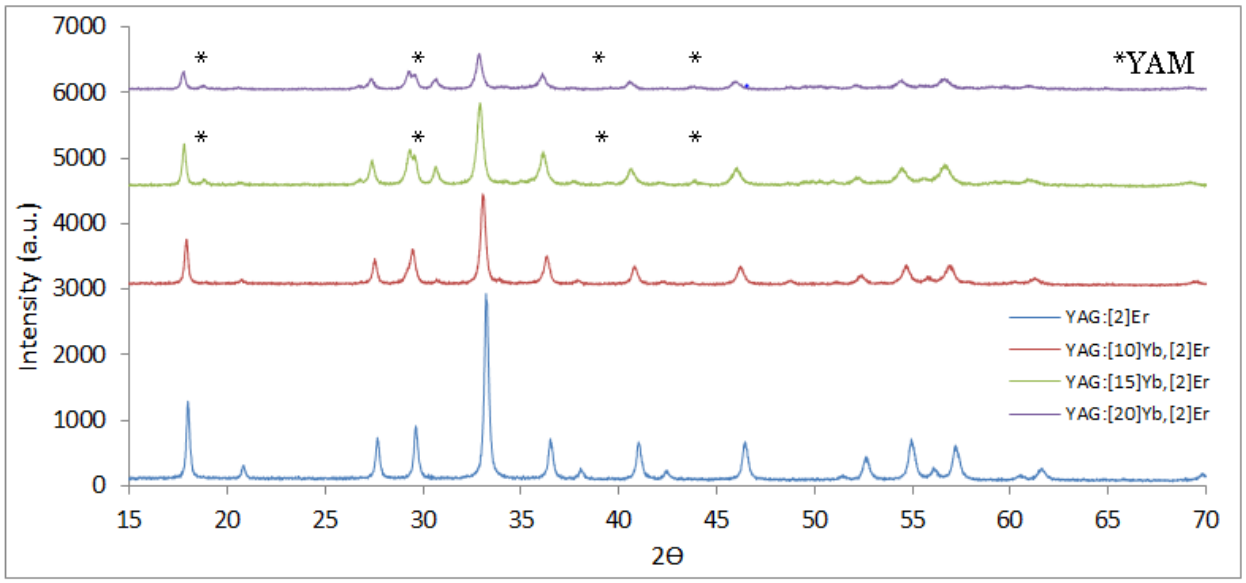

Figure 12. XRD of selected YAG:RE^{+3} with YAM peaks labeled with (*) for YAG:[15,20]Yb^{+3},Er^{+3}.

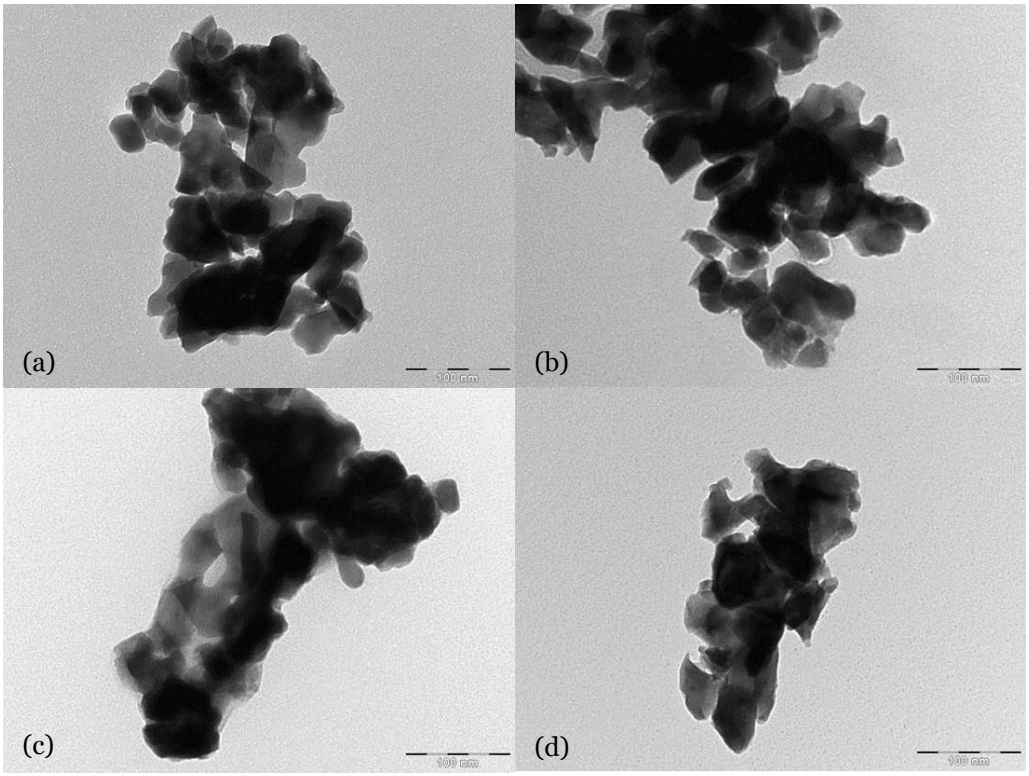

Figure 13. Selected TEM images representing (a) YAG:Er, (b) YAG:[10]Yb,Er, (c) YAG:[15]Yb,Er and (d) YAG:[20]Yb,Er.

4.3.2 Chemical Composition Analysis

Table 5 shows the compositions of the UP and composite photocatalysts determined by EDS. Examination of the data reveals proper incorporation of the Er^{+3} at loading of 1.03 +/- 0.17 atomic percent (at%) in the UPs and a doubling in [Yb^{+3}] for the YAG:[10,15,20]Yb^{+3},Er^{+3} series of UPs. A noticeable decreasing in Al and O at% can be seen as assumed [Yb^{+3}] reach above 15 mol% which correlates well with what was found from XRD in that a phase shift from $Y_3Al_5O_{12}$ to $Y_4Al_2O_9$ was observed at these [Yb^{+3}]. Y at% also peaks at the maximum Yb^{+3} loading, once again agreeing with the increase of Y:Al from 3:5 to 2:1 and Y:O from 1:4 to 4:9 resulting from a change in crystallinity. The data also confirms that mixing the various UPs, which have varying molar masses, with

titania resulted in a uniform Ti loading of 25.5 +/- 1.5 at%. This piece of information rules out enhanced or decreased rates due to comparison of composites with mixed compositions of active photocatalyst material which can often be overlooked [25].

Table 5. Chemical composition of YAG:RE^{+3} UP and TiO_2/YAG:RE^{+3} composite photocatalyst in atomic percent.

Sample	% Ti	% O	% Y	% Al	% Er	% Yb
YAG	-	65.4	13.5	21.1	-	-
YAG:Er^{+3}	-	64.5	12.9	21.5	1.1	-
YAG:[10]Yb^{+3},Er^{+3}	-	62.1	12.9	20.0	0.8	4.2
YAG:[15]Yb^{+3},Er^{+3}	-	62.0	11.0	17.6	1.0	8.4
YAG:[20]Yb^{+3},Er^{+3}	-	59.0	15.5	10.5	1.2	13.8
TiO_2/YAG	23.4	66.6	3.9	6.1	-	-
TiO_2/YAG:Er^{+3}	25.8	66.1	3.0	4.7	0.4	-
TiO_2/YAG:[10]Yb^{+3},Er^{+3}	26.7	68.6	1.5	2.3	0.1	0.8
TiO_2/YAG:[15]Yb^{+3},Er^{+3}	26.9	67.6	1.6	2.8	0.1	1.0
TiO_2/YAG:[20]Yb^{+3},Er^{+3}	24.5	71.5	1.1	1.9	0.1	0.9

4.3.3 Optical Characterization

Optical properties of the TiO_2/YAG:RE^{+3} composites were studied using DRS in the range of 350-1200 nm. In Figure 14 (a) relatively uniform reflectance peaks are seen throughout the Vis region which is expected due to a constant Er^{+3} concentration in all samples and Yb^{+3} lacking any activity throughout the Vis spectrum. Within the IR region, Er^{+3} contributions are only detectable in the TiO_2/YAG:Er^{+3} sample due to an overlap in reflectance peaks associated with Er^{+3} and Yb^{+3}. A broadening and intensification of the overlapping band correlating to the $^2F_{7/2} \rightarrow {}^2F_{5/2}$ energy transfer process of Yb^{+3} signifies successful incorporation of Yb^{+3} at increasing amounts [33]. Tauc plots of $(\alpha h\nu)^{0.5}$ vs. photon energy ($h\nu$) for the TiO_2/YAG:RE^{+3} composites are

provided in Figure 14 (b) with TiO_2 as a reference material. The E_{bg} of the materials were estimated by using Tauc's formula: [34]

$$(\alpha hv)^{\frac{2}{n}} = A(hv - E_{bg})$$

where α is the absorption coefficient, n denotes the transition state (n = 4, indirect) and A is the slope of the tangent line corresponding to the point of inflection [35]. The E_{bg} is found by locating the point of intersection on the x-axis of the tangent lines which are tabulated in Table 4. It can be seen that the addition of YAG:RE^{+3} does not have an effect on the E_{bg} of the titania photocatalyst which negates the possibility of improved or decreased reaction rates due to altering the fraction of light which has more energy than the associated E_{BG} for a given light source [3]. This being said, only photons with E_p > 3.03 eV (λ < 409 nm) have enough energy to initiate the photocatalytic process. Equivalent E_{bg} also allows for reliable comparative studies of UCL driven photocatalysis to be made in the absence of photons with $E_p > E_{bg}$ because the minimal required energy for each composite is the same. This is important to this set of experiments because one of the intentions of this study is to gain insight into the applicability of intensified PL emissions of upconverted light due the sensitization of Er^{+3} by Yb^{+3} to a commercial titania photocatalyst. Given the nature of the RE^{+3}, ETU driven photocatalysis is restricted to light within the overlapping bands found in Figure 14 (a).

Figure 15 displays the spectral bands throughout the Vis and IR regions associated with the absorption and scattering of light by Er^{+3} with peaks located at 488, 522, 654 and 968 nm. These bands are attributed to excitation from the Er^{+3} ground state $^4I_{15/2}$ to the excited states $^4F_{7/2}$, $^4S_{3/2}$, $^4F_{9/2}$, and $^4I_{11/2}$ respectively [11]. The

significance of these bands is that they are located in the most intense region of the solar spectrum which allows for greater probability of upconversion luminescence to occur when solar radiation is used as the energetic light source for photocatalytic reactions [10]. The upconversion luminescence properties of RE^{+3} have been studied thoroughly over the last couple decades and low intensity UV emissions from Vis and IR excitation sources of Er^{+3} and Yb^{+3} doped/co-doped UP has been well documented [11] [25] [27] [33]. The PL spectra in Figure 16 confirms the generation of photons with $E_p > E_{bg}$ through Vis to UV upconversion luminescence by the YAG:Er^{+3} UP. The emission bands about 390 nm (3.18 eV) and 403 nm (4.07 eV) are attributed to the $^4G_{11/2} \rightarrow {}^4I_{15/2}$ and $^2P_{3/2} \rightarrow {}^4I_{13/2}$ transitions respectively and were obtained under 488 nm excitation [36].

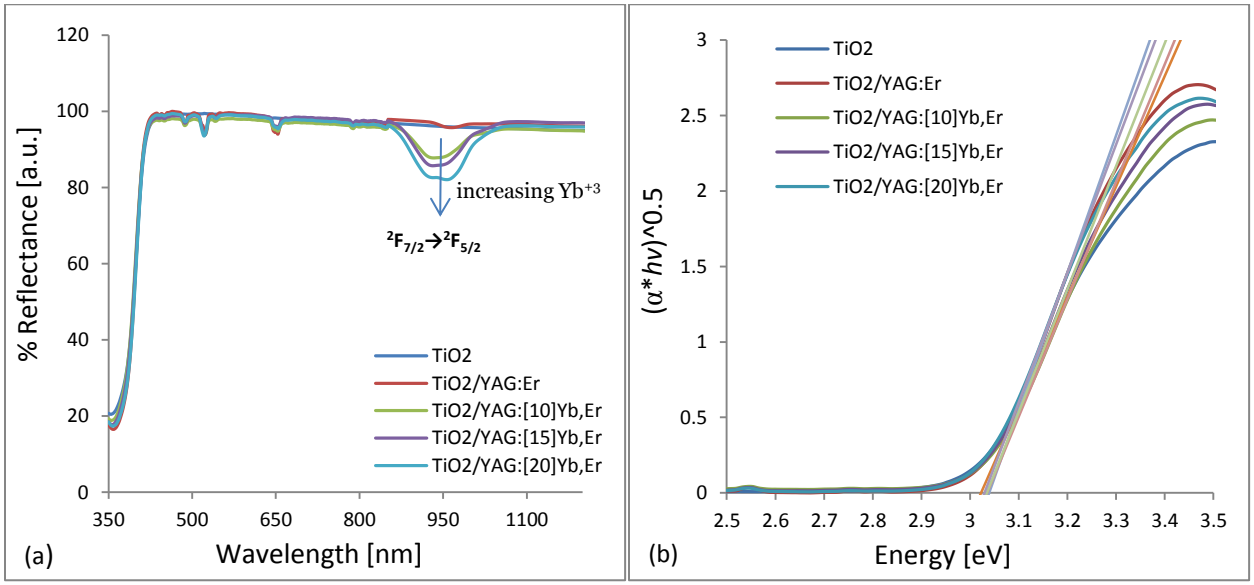

Figure 14. (a) UV-Vis-IR DRS of TiO_2/YAG:RE^{+3} composites with corresponding Yb^{+3} energy transition and (b) Tauc plot.

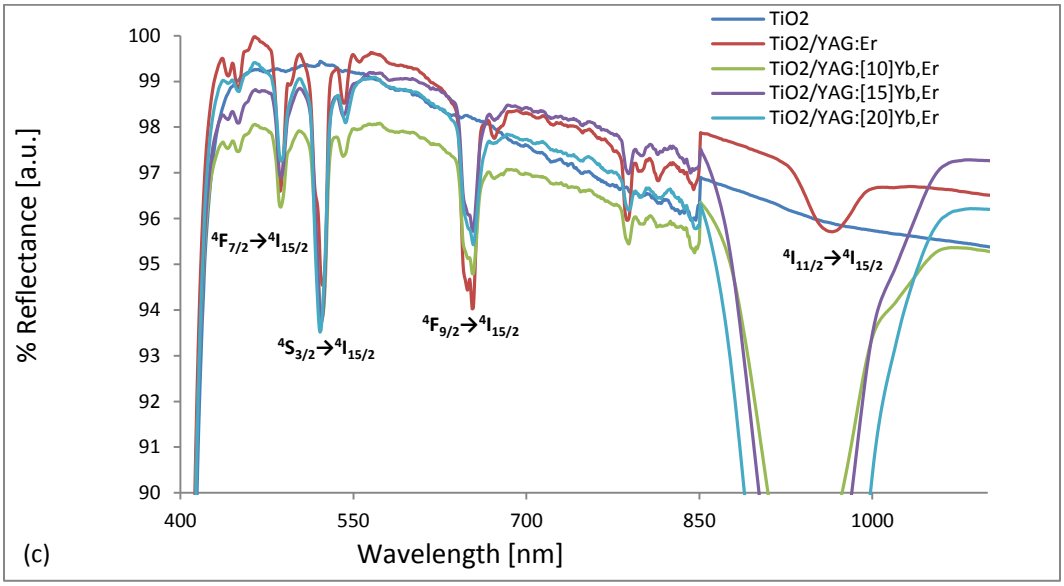

Figure 15. UV-Vis-IR DRS of TiO_2/YAG:RE composites with Er^{+3} energy transitions.

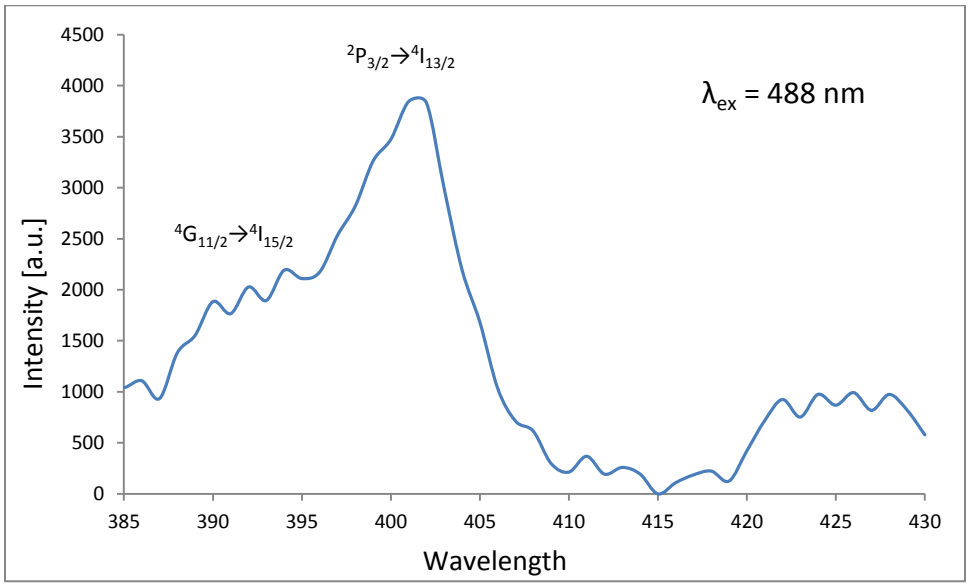

Figure 16. PL spectra of YAG:Er^{+3} resulting from 488 nm excitation.

4.3.4 Photocatalytic Activity

RB dye was chosen as a model pollutant for the photocatalytic studies due to its neutral nature and resistance to UV-Vis photo bleaching. It has been widely reported that the hydroxyl radical attack dominates the degradation process when compared to direct oxidation or reduction of the dye due to a charge separation associated with an excited semiconductor molecule and is supported by various hydroxyl scavenger studies [20]. In both the UV and UV-Vis studies a constant weight loading of 0.06 g titania was used as the UP is not known to provide any means of dye degradation. This was confirmed by performing experiments without any titania present which resulted in a negligible reduction in dye concentration. During these studies it was also important to maintain a constant initial supernatant dye concentration prior to activating the photocatalyst due to the first order dependence of the degradation rate on the model pollutant's concentration. This required preliminary adsorption studies which are not reported in this document.

Table 6. Φ_{RB} and k'_{RB} of TiO_2/YAG:RE^{+3} photocatalyst under UV, UV-Vis and IR conditions.

Sample	k'_{UV} [mL/(g*s)]	$\Phi_{RB\ UV\text{-}Vis}$ [%]	k'_{IR} [mL/(cm²*s)]
TiO_2	9.42	0.0589	-
YAG	0.38	-	-
TiO_2/[10]YAG	17.22	-	-
TiO_2/[5]YAG:Er^{+3}	-	0.0689	-
TiO_2/[10]YAG:Er^{+3}	18.27	0.0774	0.00581
TiO_2/[15]YAG:Er^{+3}	-	0.0626	-
TiO_2/YAG:[10]Yb^{+3},Er^{+3}	-	0.0763	-
TiO_2/YAG: [15]Yb^{+3},Er^{+3}	20.69	0.0837	.00311
TiO_2/YAG:[20]Yb^{+3},Er^{+3}	-	0.0752	-

To determine the optimal [YAG:RE^{+3}], a series of composites with 5, 10 and 15 mol% YAG:Er^{+3} were studied under 'daylight' conditions resulting in a maximum

degradation rate of -2.36 E-6 moL RB/(g*min) at 10 mol%. This correlates well with other findings which reported maximum degradation rates of titania/UP composites near a mass ratio of 1:1, ours being closer to 0.8:1 [26]. Building upon these results, the composites of varying [Yb^{+3}] were subjected to the same 'daylight' study with a [YAG:RE^{+3}] of 10 mol%. Initially the introduction of Yb^{+3} had a negative effect on the observed rate constant, reducing it by 3.1% at a [Yb^{+3}] of 10 mol% as seen in Table 6. However, when the [Yb^{+3}] was raised from 10 to 15 mol% in the YAG:RE^{+3} the degradation rate increased to -2.52 E-6 moL RB/(g*min) which is a 6.8% increase from that which was observed by the optimal YAG:Er^{+3} composite. Interesting enough the trend did not continue on to the next increase in [Yb^{+3}] which again had a negative effect on the TiO_2/[10]YAG:RE^{+3} ability to degrade the dye, but still improved upon bare P25 titania by 32%. Figure 17 (a) and (b) display the two separate progressions of varying [YAG:Er^{+3}] and [Yb^{+3}] while Figure 17 (c) reveals the trend found in the UV-Vis studies with respect to the investigated mol%. It is our theory that an increase in degradation rate is observed when comparing the TiO_2/[10]YAG:Er^{+3} and TiO_2/YAG:[15]Yb^{+3},Er^{+3} composites is due to the slight shift in crystalline phase of the Y_2O_3-Al_2O_3 binary system from garnet to monoclinic, which may improve upon the suppression of recombination rates of e^-/h^+ pairs as in many heterostructured systems [29]. A rapid increase and decline of this electronic enhancement mechanism, as found in our study of mixed phase YAG:Yb^{+3},Er^{+3}, agrees with similar reported trends in which such charge separation enhancements are largely dependent on phase composition [29].

As a means to help support this claim, similar studies were conducted with bare P25 titania and the TiO_2/[10]YAG, TiO_2/[10]YAG:Er^{+3}, and TiO_2/YAG:[15]Yb^{+3},Er^{+3} composites under UV conditions. The reasoning behind these trials was to rule out any

possibility of enhancement due to upconversion luminescence and to study enhancement due to suppressed e^-/h^+ recombination rates and increases in dye concentration near the catalysts surface from improved adsorption capabilities of the Y-Al oxide. The results of this study are shown in Figure 18and it can be seen that once again the TiO_2/YAG:[15]Yb^{+3},Er^{+3} composite had the largest observed rate constant. Differing from the UV-Vis study, the incorporation of 15 mol% Yb^{+3} increased the degradation rate by 13.2% rather than 6.8% when compared to the TiO_2/[10]YAG:Er^{+3} composite and by 120% rather than only 46.9% when compared to bare P25 titania. This suggests that the enhancement seen during the UV-Vis trials was dominated by electronic interactions of the titania photocatalyst and YAG:RE^{+3} and increased dye concentrations near the catalysts surface opposed to enhancement found from UCL driven photocatalysis, which requires Vis to UV UCL to occur. These claims are supported by the fact that the TiO_2/YAG enhanced the observed reaction rate by 83% when compared to pure titania but when pure YAG was tested alone, no reaction rate was observed.

To cover all possible mechanisms of enhancements applicable to the TiO_2/YAG:RE^{+3} composite under solar radiation, a separate study was done in a batch-type reactor in which only a fraction of the reaction liquid was exposed to light while the rest recirculated using a pump. The reactor vessel was equipped with two IR LEDs which produced a spectrum centered at 940 nm with a bandwidth (FWHM) of 37 nm. Utilization of this light source improves upon sensitization studies intended to be applied to solar photocatalyst as it encompasses the entire overlapping spectra of the Yb^{+3} and Er^{+3} found from DRS rather than using a laser which supplies a much narrower bandwidth. Normalization of the data also differed from the UV and UV-Vis

trials as the illuminated surface areas were used as a normalization factor opposed to the weight of titania present. This route was backed up by performing a thickness test of the immobilized films and it was found that additional layers of composite did not increase reaction rates due to the inability of photons to penetrate any further through the films, justifying normalization by surface area. Initially a comparison was made between the TiO_2/[10]YAG:Er^{+3} and TiO_2/YAG:[15]Yb^{+3},Er^{+3} composites and what was found was that the addition of Yb^{+3} severely retarded the degradation of RB dye, the reason being an overabundance of sensitizing ions which results in self-quenching by cross-relaxation and cooperative UCL of neighboring excited Yb^{+3} rather than the desired nonradiative transfer of energy to ground state and excited Er^{+3} referred to as sensitization [10].

To address this issue a separate series of composites were synthesized with Yb^{+3}:Er^{+3} of 05:1, 1:1 and 1.5:1 to be tested as previously reported materials with low Yb^{+3}:Er^{+3} showed increased IR to Vis UCL emission [33]. Here it was found that even at low Yb^{+3}:Er^{+3}, increased degradation rates due to improved UV emissions from the addition of a sensitizing ion proves unlikely to occur. As seen in Figure 19 the addition of 1 mol% Yb^{+3} does not affectively change the observed degradation rate and the addition of 2 mol% Yb^{+3} reduces the rate by 9%. These results seem to agree with what has been previously reported in regards to Yb^{+3}-Er^{+3} co-doped materials in that the sensitization of Er^{+3} by Yb^{+3} typically results in increased red and green UCL emissions and claims of improved IR to UV emissions have been limited to Tm^{+3}/Ho^{+3}-Yb^{+3} co-doped systems [27] [34].

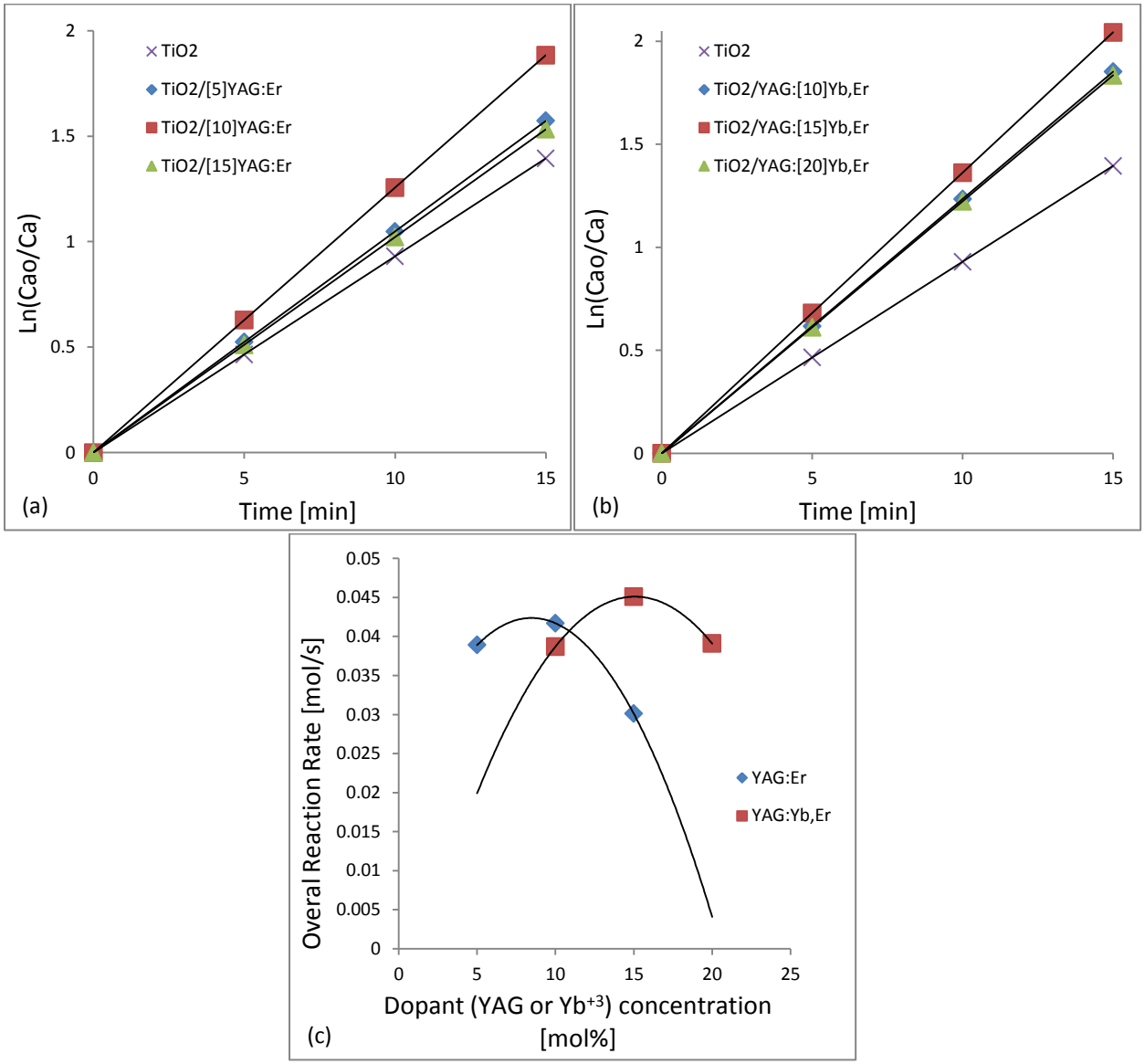

Figure 17. RB degradation under UV-Vis conditions for (a) TiO_2/[5,10,15]YAG:Er^{+3} and (b) TiO_2/YAG:[10,15,20]Yb^{+3},Er^{+3} composites. (c) Reaction rate vs dopant concentration curves for varying dopant concentrations.

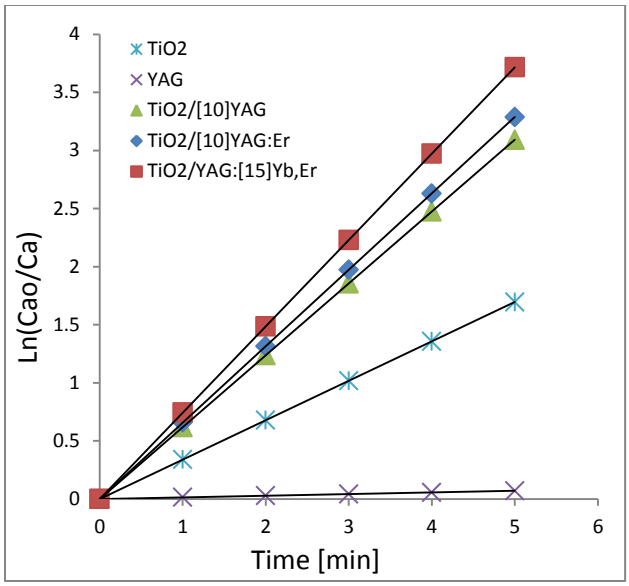

Figure 18. RB degradation under UV conditions.

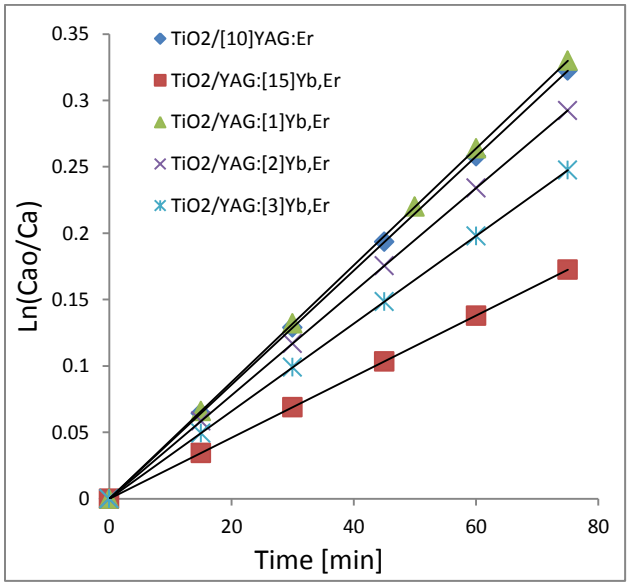

Figure 19. RB degradation under IR conditions.

4.4 Conclusions

Improved photocatalytic function of titania by means of incorporation of an UP has been thoroughly studied with regards to solar applications. Simple and reproducible synthesis techniques were utilized to both synthesize the YAG:RE^{+3} UPs and TiO_2/YAG:RE^{+3} composites. EDS was used to confirm the chemical compositions of the synthesized materials which returned proper compositions for the varying composites. Observing the photocatalytic degradation of RB under UV, UV-Vis and IR conditions with varying [Yb^{+3}] resulted in an optimal composite composition of TiO_2/[10]YAG:[15]Yb^{+3},Er^{+3} for applications in which solar radiation is used as the energetic light source in semiconductor photocatalysis. The enhancement gained by incorporation of the UP with the titania photocatalyst came in three forms: creation of more UV photons by means of UCL, improved electron-hole pair recombination rates due to electronic interactions and by increased contaminant adsorption near the catalysts surface. It is noteworthy, as it was the intentions of the study to investigate the applicability of Yb^{+3} as the sensitizing ion to Er^{+3} for increased UV UCL emissions, that the increase in photocatalytic activity was largely dominated by only two of the previously mentioned routes: electronic interactions and increased contaminant adsorption. Under UV-Vis conditions, Yb^{+3} and Er^{+3} do not have any overlapping absorption bands as shown by DRS and enhancement from an increase in UV UCL emissions related to the ETU process was not found under the proper IR conditions. Instead, the enhancement found by introducing Yb^{+3} into the YAG:Er^{+3} UP is credited to a slight phase shift in the host material from garnet to monoclinic and it is (our) theory that the mixed phased Y-Al oxide offers slightly better charge separation enhancement

due to an increase in material defects and possible band structures as the adsorption capacities of the YAG:RE^{+3} UPs did not differ from composition to composition.

CHAPTER 5: CONCLUSIONS AND FUTURE OUTLOOK

A study of employing nanomaterials which possess unique optical properties to obtain enhanced activity of a titania photocatalyst under solar radiation has been presented and discussed. It is the objective of this final chapter to: give a comprehensive reasoning to the results discussed in chapters 3 and 4, offer a conclusion to the applicability Ag-Pd core-shell nanoparticles (Ag-Pd NP) and Yb^{+3}-Er^{+3} co-doped Y-Al oxides (YAG:RE^{+3}) have to wastewater remediation, and to discuss some of the novelty of the research and its impact to future work.

Enhancement from the addition of plasmonic NP, namely Ag nanocubes (NC) and a novel Ag-Pd NP, to a titania photocatalyst was initially investigated in a shallow dish, batch reactor using fluorescent light bulbs which produced a spectrum similar to the daylight spectrum. This first step was taken to probe into the possibility of testing the TiO_2/NP composites in a manner more often used when performing liquid phase, photocatalytic reactions. A series of increasing NP wt% revealed a decreasing trend in the observed degradation rates when compared to the bare titania photocatalyst. The reduction in degradation rates at loadings of 0.3, 1.0, and 10 wt% Ag NC were attributed to: a reduction in catalyst surface area due to testing all samples at equal titania loadings opposed to equivalent surface areas, differences in mixing efficiencies due to adding a much denser material, and reflection of light at the liquid surface from colloidal Ag NC. An interesting result was achieved however in that when comparing equal loadings of 1.0 wt% Ag NC and Ag-Pd NP, the TiO_2/[1.0]Ag-Pd NP composite achieve a degradation

rate 1.2 times that of the TiO_2/[1.0]Ag NC composite. From the results in this set of experiments it was reasoned that TiO_2/NP composites are not well suited for applications in classic shallow dish batch reactors.

Building upon these results, a novel approach to the experimental design was taken in that a stable, layered film and composite film were tested in a recirculating, batch type reactor. In previously reported experimental findings, photocatalytic rates were obtained by measuring the de-coloration of a titania film in air and it was this area at which the experimental design was improved. A stainless steel reactor was fabricated, upon which two high-powered LEDs were mounted for selectable radiation frequency, which housed a glass substrate that had an immobilized TiO_2+NP system or a TiO_2/NP composite film. The two arrangements were tested under UV conditions and initial results revealed that adding a layer of Ag NC under a bare titania film doubled the observed degradation rate. The overserved enhancement did not match the previously reported enhancement factor of 3.9 but evidence of stability in recirculating, liquid phase reactions was shown [7]. Comparison of the TiO_2+Ag NC and TiO_2+Ag-Pd NP films revealed a reduction in enhancement due to a loss in plasmonic interactions associated with the corners and edges of the Ag core, resultant of the addition of a Pd shell as shown through UV-Vis spectroscopy.

For completion of the study on plasmonic enhancement, a series of composites with even lower NP wt% loadings were tested using the batch type reactor. TiO_2/NP composites with NP loadings of 0.05 and 0.1 wt% Ag NC and Ag-Pd NP were applied to glass slides using an air brush which utilized lab air as the propellant. An initially thickness studied ruled out the possibility of increased rates due to variations in compared film thickness by showing that the upper limit of film thickness with respect

to the magnitude of observed reaction rate was met after one application of the TiO_2/NP slurry. After ruling this important factor out, the results from the final set of experiments showed that at a loading of 0.05 wt%, the TiO_2/[0.05]Ag-Pd NP film performed 10% better than the TiO_2/[0.05]Ag NC film, which is the first time an enhancement was found due to the addition of the Pd shell that was also an improvement on the bare titania reference. The resulting enhancement is concluded to be based off of a lone electronic effect commonly associated with Pd nanoparticles in which their naturally positive valences suppress rates of recombination in neighboring excitons, as plasmonic enhancement must be ruled out due to not observing any in the TiO_2/Ag NC film. Having made those last statements, increasing the NP loading to 0.1% resulted in equal rates to that which was seen by the TiO_2/[0.05]Ag-Pd NP film by both the TiO_2/[0.1]Ag NC and TiO_2/[0.1]Ag-Pd NP. Reasoning for this can be drawn from the extinction spectrums in that the plasmonic interactions due to the corners and edges of the Ag NC provided more intense interactions with light provided by the UV LEDs used in the experiment. The 0.1 wt% Ag-Pd NP system, which had a reduction in these shoulders, was able to reach the same photocatalytic rate due to the electronic enhancement from the Pd shell.

Enhancement by the addition of YAG:RE^{+3} to a titania photocatalyst was examined to gain insight into the applicability the sensitization of Er^{+3} by Yb^{+3} had to the enhancement received via the upconversion luminescence (UCL) phenomena under solar radiation. Initially it was found that a loading of 10 mol% YAG:Er^{+3} optimized the observed degradation rate under similar batch reactor conditions initially used in the plasmonic enhancement study, the difference being the model pollutant and catalyst density. These results agreed with what was previously report for TiO_2/YAG:Er^{+3}

composites [26]. The observed enhancement of 37% has been concluded to be from: an increase in UV photons due to Vis-UV UCL, improved recombination rates from electronic interactions between Er^{+3} and excitons near the photocatalyst's surface, and increased contaminant concentrations near the catalyst surface due to the higher adsorption efficiency offered by the single phase Y-Al oxide. Following these results, a series of YAG:RE^{+3} were synthesized with increasing amounts of Yb^{+3} and were subjected to the same experimental trials. Further enhancement was found when testing the composite which had an assumed Yb^{+3} concentration of 15 mol% which was concluded to be from improved recombination rates resultant of intensified electronic interactions between areas with defects in the now mixed phased YAG:RE^{+3} and neighboring excitons. It has also been made clear that enhanced UV UCL due to the energy transfer upconversion (ETU) process are not relevant here due to no overlapping in the UV-Vis region was found from diffuse reflectance spectroscopy (DRS).

Tests were also conducted under UV conditions in the same batch reactor as the UV-Vis trials for the TiO_2/YAG:RE^{+3} composites. In these set of experiments a TiO_2/[10]YAG composite was studied as a reference which in fact improved upon the observed degradation rate seen by the bare titania by a factor 1.8. This enhancement was ruled to be from increased contaminant concentrations near titania's surface due to the heightened adsorption capacity of the composite. A trial was also run using on YAG and it was shown that UV light and YAG do not result in any actions which degrade the pollutant. The largest contribution taken from this study was that enhancement of the TiO_2/YAG:[15]Yb^{+3},Er^{+3} under UV conditions was larger when compared to both bare titania and the TiO2/YAG:Er^{+3} composite than what was seen under UV-Vis conditions. The reasoning for this was that enhancement seen in the UV-Vis trials must have been

dominated by the electronic and adsorption effects opposed to any enhancement from Vis-UV UCL.

To address the intentions of investigating the applications of the ETU process between Yb^{+3} and Er^{+3} experimental trials were conducted in the batch type reactor utilizing high-powered IR LEDs. Initial trials were conducted on the substrates with TiO_2/YAG:Er^{+3} and TiO_2/YAG:[15]Yb^{+3},Er^{+3} films and it was quickly realized that such high Yb^{+3} concentrations did not result in increased IR-UV emissions from the ETU process. After synthesizing a series of composites with Yb^{+3}:Er^{+3} of 0.5:1, 1:1 and 1.5:1 to examine newly reported Yb^{+3}:Er^{+3} which show enhanced sensitization in phosphate glass, photocatalytic testing was conducted under the same IR conditions which resulted in a decreasing trend in degradation rate with in increasing Yb^{+3}:Er^{+3} [33]. Upon obtaining these results it was determined that there were no realizable application of ETU process, with respect to Yb^{+3} and Er^{+3}, to a commercially available titania photocatalyst under solar radiation. This conclusion was drawn due to the weaker intensities of applicable light provided by solar radiation which will result in even fewer emissions of UV photon from any type of UCL process than what was seen in our batch type experiments and that typical reports of increased UCL emission due to Yb^{+3} sensitizing Er^{+3} are reported in the green and red spectrums and not UV.

In summary of the manuscript, novelty to the scientific community has been offered in the form of: a novel Ag-Pd core-shell NP synthesis which produces a NP which retains the plasmonic properties of its cubic Ag core while offering the catalytic properties of Pd: an improved approach to studying plasmonically enhanced photocatalysis that allows proper comparison of obtained results to be made to the field of wastewater remediation, and an improved approach to studying ETU by the use of

high-powered LEDs which produce spectra that completely cover the overlapping optical absorption bands associated with the sensitizing and acceptor ions. Although limited photocatalytic improvement has been shown for the Tio_2/Ag-Pd NP, the design and optimization of the successive reduction synthesis has opened doors in other fields such as sensors and photo assisted electro chemistry to explore the use of the newly synthesized material. The same can be said about the improved experimental set-up with regards to plasmonically enhanced and upconversion enhanced photocatalytic studies. Although the results do not show drastic improved photocatalytic rates, the newly fabricated reactor set up allows for greater control and variability in the impinging photon flux at the catalysts surface which can allow for more elaborate studies to be conducted. Having said this, future work that stems from this study includes but is not limited to: the use of the recirculating batch type system for studies which vary the intensity of the LED to match what is available from solar radiation at similar wavelengths, investigating the other possible fields the novel Ag-Pd NP have applications too, and further testing of the Ag-Pd NP with better characterization techniques and more variations in shell thicknesses.

REFERENCES

[1] J. Crittenden, Water Treatment Principles and Design, Hoboken, NJ: Wiley, 2005.

[2] H. Choi, S. Al-Abed, D. Dionysiou, E. Stathatos and P. Lianos, "TiO2-Based Advanced Oxidation Nanotechnologies for Water Purification and Reuse," *Sust. Sci. and Eng.,* no. 2, pp. 229-254, 2010.

[3] S. Ahmed, M. Rasul, W. Martens, R. Brown and H. M, "Heterogeneous photocatalytic degradation of phenols in wastewater: A review on current status and developements," *Desal.,* no. 261, pp. 3-18, 2010.

[4] L. Sun and J. Bolton, "Determination of the Quantum Yield for the Photochemical Generation of Hydroxyl Radicals in TiO2 Suspensions," *J. Phys. Chem.,* no. 100, pp. 4127-4134, 1996.

[5] M. Cortie and A. McDonagh, "Synthesis and Optical Properties of Hybrid and Alloy Plasmonic Nanoparticles," *Chem. Rev.,* no. 111, pp. 3713-3795, 2011.

[6] A. Haes and R. Duyne, "A Nanoscale Optical Biosensor: Sensitivity and Selectivity of an Approach Based on the Localized Surface Plasmon Resonance Spectroscopy o Triangular Silver Nanoparticles," *Jour. Am. Chem. Soc.,* no. 124, pp. 10596-10604, 2002.

[7] P. Christopher, D. Ingram and S. Linic, "Enhancing Photochemical Activity of Semiconductor Nanoparticles with Optically Active Ag Nanostructures: Photochemistry Mediated by Ag Surface Plasmons," *J. Phys. Chem. C,* no. 114, pp. 9173-9177, 2010.

[8] B. Wiley, Y. Sun, B. Mayers and Y. Xia, "Shape-Controlled Synthesis of Metal Nanostructures: The Case of Silver," *Chem. Eur J.,* no. 11, pp. 454-463, 2005.

[9] J. Gong, F. Zhou, Z. Li and Z. Tang, "Controlled synthesis of non-epitaxially grown Pd@Ag core-shell nanocrystals of interesting optical performance," *The Royal Society of Chemistry,* no. 49, pp. 4379-4381, 2013.

[10] F. Auzel, "Upconversion and Anti-Stokes Processes with f and d Ions in Solids," *Chem. Rev.,* no. 104, pp. 139-173, 2004.

[11] G. De, W. Qin, J. Zhang, J. Zhang, Y. Wang, C. Coa and Y. Cui, "Upconversion luminescence properties of Y2O3:Yb,Er nanostructures," *J. Lum.,* no. 119-120, pp. 258-263, 2006.

[12] Q. Zhang, W. Li, L. Wen, J. Chen and Y. Xia, "Facile Synthesis of Ag Nanocubes of 30 to 70 nm in Edge Length with CF3COOAg as a Precursor," *Chem.,* no. 16, pp. 10234-10239, 2010.

[13] S. Hassanzadeh-Tabrizi, "Synthesis and luminescence properties of YAG:Ce nanopowder prepared by the Pechini method," *Adv. Pow. Tech.,* vol. 23, pp. 324-327, 2012.

[14] X. Lu, M. Rycenga, S. Skrabalak, B. Wiley and Y. Xia, "Chemical Synthesis of Novel Plasmonic Nanoparticles," *Annu. Rev. Phys. Chem.,* no. 60, pp. 167-192, 2009.

[15] F. Pincella, K. Isozaki and K. Miki, "A visible light-driven plasmonic photocatalyst," *Light: Sci. and Appl,* no. 3, pp. 1-6, 2014.

[16] K. Awazu, M. Fujimaki, C. Rockstuhl, J. Tominaga, H. Murakami, Y. Ohki, N. Yoshida and T. Watanabe, "A Plasmonic Photocatalyst Consisting of Silver Nanoparticles Embedded in Titanium Dioxide," *J. Am. Chem. Soc.,* no. 130, pp. 1676-1680, 2008.

[17] S. Mogal, V. Gandhi, M. Mishra, S. Tripathi, T. Shripathi, P. Joshi and D. Shah, "Single-Step Synthesis of Silver-Doped Titanium Dioxide: Influence of Silver on Structural, Textural and Photcatalytic Properties," *Ind. and Eng. Chem. Res.,* no. 53, pp. 5749-5758, 2014.

[18] A. Tedsree, T. Li, S. Jones, C. Chan, K. Yu, P. Bagot, E. Marquis, G. Smith and S. Tsang, "Hydrogen production from formic acid decomposition at room temperature using a Ag-Pd core-shell nanocatalyst," *Nature Nanotech,* no. 6, pp. 302-307, 2011.

[19] P. Ameta, A. Kumar, M. Paliwal, R. Ameta and R. Malkani, "Photocatalytic Bleaching of Rose Bengal by Some Coloured Semiconducting Oxides," *Bull. of the Cat. Soc. of Ind.,* no. 6, pp. 130-135, 2007.

[20] S. Sharma, R. Ameta, R. Malkani and S. Ameta, "Photocatalytic degradation of Rose Bengal using semiconducting zinc sluphide as the photocatalyst," *J. of the Serb. Chem. Soc.,* no. 78, pp. 897-905, 2013.

[21] R. Kumawat, I. Bhati and R. Ameta, "Role of some metal ions in photocatalytic degradation of Rose Bengal dye," *Ind. J. of Chem. Tech.,* no. 19, pp. 191-194, 2012.

[22] N. Mittal, A. Shah, P. Punjabi and V. Sharma, "Photodegradation of rose bengal using MnO2 (Manganese dioxide)," *Rasayan J. Chem,* no. 2, pp. 516-520, 2009.

[23] W. Li, D. Li, Y. Lim, P. Wang, W. Chen, X. Fu and Y. Shao, "Evidence for the Active Species Involved in the Photodegradation Process of Methyl Orange on TiO2," *J. of Phys. Chem. C,* no. 116, pp. 3552-3560, 2012.

[24] S. Obregon, A. Kubacka, M. Fernandez-Garcia and G. Colon, "High-performacne Er-TiO2 system: Dual upconversion and electronic role of the lanthanide," *J. Cat,* no. 299, pp. 298-306, 2013.

[25] J. Reszczynska, T. Grzyb, J. Sobczak, W. Lisowski, M. Gazda, B. Ohtani and A. Zaleska, "Visible light activity of rare earth metal dope (Er, Yb or Er/Yb) titania photocatalyst," *App. Cat B: Env.,* no. 163, pp. 40-49, 2015.

[26] G. Feng, S. Liu, Z. Xiu, Y. Zhang, J. Yu, Y. Chen, P. Wang and X. Yu, "Visible Light Photocatalytic Activities of TiO2 Nanocrystals Doped with Upconversion Luminescence Agent," *J. Phys. Chem C,* no. 112, pp. 13692-13699, 2008.

[27] X. Wu, S. Yin, Q. Dong, B. Liu, Y. Wang, T. Sekino, S. Lee and T. Sato, "UV, visible and near-infrared lights induced NOx destruction activity of (Yb,Er)-NaYF4/C-TiO2 composite," *Sci Rep,* no. 2918, pp. 1-8, 2013.

[28] W. Wang, M. Ding, C. Lu, Y. Ni and Z. Xu, "A study on upconversion UV-Vis-NIR responsive photocatalytic activity and mechanisms of hexagonal phase NaYF4:Yb,Tm@TiO2 core-shell structured photocatalyst," *App. Cat. B: Env.,* no. 144, pp. 379-385, 2014.

[29] S. Obregon and G. Colon, "Heterostructured Er doped BiVO4 with exceptional photocatlalytic perfomance by cooperative electronic and luminescence sensitization mechanism," *App. Cat. B: Env.,* no. 158-159, pp. 242-249, 2014.

[30] E. Garskaite, D. Jasaitis and A. Kareiva, "Sol-gel prepartion and electrical behaviour of Ln:YAG (Ln = Ce, Nd, Ho, Er)," *J. Serb. Chem. Soc.,* vol. 68, pp. 677-684, 2003.

[31] P. Rai, M. Song, H. Song, J. Kim, Y. Kim, I. Lee and Y. Yu, "Synthesis, growth mechanism and photoluminescence of monodispered cubic shape Ce doped YAG nanophosphor," *Cerm Int.,* no. 38, pp. 235-242, 2012.

[32] N. Karkada, D. Porob, P. Kumar and A. Setlur, "Preparation and Luminescence of BaSi6N8O:Eu Oxynitride Phosphor," *Electro. Chem. Soc. Trans.,* no. 31, pp. 41-50, 2009.

[33] F. Huang, X. Liu, Y. Ma, S. Kang, L. Hu and D. Chen, "Origin of near to middle infrared luminescence and energy transfer process of Er3+/Yb3+ co-doped fluorotellurite glass under different excitations," *Sci. Rep.,* 2015.

[34] X. Guo, W. Di, C. Chen, C. Liu, X. Wang and W. Qin, "Enhanced near-infrared photocatalysis of NaYF:Yb,Tm/CdS/TiO2 composites," *Dalt. Trans.,* no. 43, pp. 1048-1054, 2014.

[35] M. Servos, A. Hu and A. Apblett, "Nanotechnology for Water Treatment and Purification," *Lect. Notes in Nano Sci and Tech,* vol. 22, pp. 59-60, 2014.

[36] X. Wang, G. Shan, K. Chao, Y. Zhang, R. Liu, L. Feng, Q. Zeng, Y. Sun, Y. Liu and X. Kong, "Effects of Er concentration on UV/blue upconverted luminescence and a three-photon process in the cubic nanocrystalline Y2O3:Er," *Mat. Chem. and Phys.,* no. 99, pp. 370-374, 2006.